The Slow Dynamics of Two-Spike Solutions for the Gray-Scott and Gierer-Meinhardt Systems: Competition and Oscillatory Instabilities

Wentao Sun*, Michael J. Ward†, Robert Russell‡

Abstract

The dynamics and instability mechanisms of both one and two-spike solutions to the Gierer-Meinhardt (GM) and Gray-Scott (GS) models are analyzed on a bounded one-dimensional spatial domain. For each of these non-variational two-component systems, the semi-strong spike-interaction limit where the ratio $O(\varepsilon^{-2})$ of the two diffusion coefficients is asymptotically large is studied. In this limit, differential equations for the spike locations, with speed $O(\varepsilon^2) \ll 1$, are derived. To determine the stability of the spike patterns, nonlocal eigenvalue problems, which depend on the instantaneous spike locations, are derived and analyzed. For these nonlocal eigenvalue problems, it is shown that eigenvalues can enter into the unstable right half-plane along either the real axis or through a Hopf bifurcation, leading to either a competition instability or an oscillatory instability of the spike pattern, respectively. Competition instabilities occur only for two-spike patterns, and numerically are shown to lead to the annihilation of a spike. Oscillatory instabilities occur for both one and two-spike solutions. For two-spike solutions this instability typically synchronizes the oscillations of the spike amplitudes. Since the nonlocal eigenvalue problems depend on the instantaneous spike locations, the key feature of these instabilities are that they can be dynamic in nature and can be triggered at some point during the slow evolution of a spike pattern that is initially stable at $t = 0$. The asymptotic theory is compared with full numerical simulations and previous theoretical results.

1 Introduction

Since the pioneering work of Turing [40], there have been many studies determining the conditions for the onset of instabilities of spatially homogeneous patterns in reaction-diffusion systems. Various types of weakly nonlinear theories, typically leading to amplitude equations or to the complex Ginzburg-Landau equation, have been used to study the weakly nonlinear development of these Turing instabilities. Many instability mechanisms in the weakly nonlinear regime have been identified, including, Hopf bifurcations, Eckhaus and zigzag instabilities, etc. A survey of such results in diverse physical settings is given in [1].

However, in the singularly perturbed limit, many reaction-diffusion systems allow for the existence of steady-state, or time-dependent, spatially localized solutions. In this class of solutions, spike patterns

*Department of Mathematics, Simon Fraser University, Vancouver, Canada, and School of Mathematics and Systems Science, Shandong University, China

†Department of Mathematics, University of British Columbia, Vancouver, Canada V6T 1Z2, (corresponding author)

‡Department of Mathematics, Simon Fraser University, Vancouver, Canada

are those where various components of the solution concentrate, or localize, at certain points in the domain. In contrast to the well-developed theory for the stability of spatially homogeneous solutions, there are many open problems regarding the instabilities and dynamics of spatially localized patterns. In his survey chapter on pattern formation (cf. [21]), Knobloch remarks that "The question of stability of finite amplitude structures, be they periodic or localized, and their bifurcation is a major topic that requires new insights". Notable exceptions, where the theory for localized solutions is well-advanced, are variational problems that admit a gradient flow characterization (cf. [11]), and certain special systems such as the Fitzhugh-Nagumo model (see [12] and the references therein).

In this context, we study the dynamics and instability mechanisms of certain spike-type solutions to the Gierer-Meinhardt (GM) and Gray-Scott (GS) models. For each of these two-component reaction-diffusion systems with no known variational structure, we consider the semi-strong spike-interaction limit where the ratio of the two diffusion coefficients is asymptotically large. In this limit, where only one component of the system localizes, we will analyze the dynamics and stability of one-spike and two-spike symmetric quasi-equilibrium solutions on a bounded one-dimensional spatial domain.

The Gray-Scott (GS) system (cf. [14]) models an irreversible reaction in a gel reactor where the reactor is maintained in contact with a reservoir of one of the two chemical species. In dimensionless variables, it can be written as (cf. [28], [17])

$$v_t = \varepsilon^2 v_{xx} - v + Auv^2\,, \quad -1 < x < 1\,, \quad t > 0\,; \qquad v_x(\pm 1, t) = 0\,, \tag{1.1a}$$

$$\tau u_t = Du_{xx} + (1-u) - uv^2\,, \quad -1 < x < 1\,, \quad t > 0\,; \qquad u_x(\pm 1, t) = 0\,. \tag{1.1b}$$

Here $A > 0$, $D > 0$, $\tau > 1$, and $\varepsilon \ll 1$. In the low feed-rate regime, defined by $A = O(\varepsilon^{1/2})$, we introduce

$$A = \varepsilon^{1/2}\mathcal{A}\,, \qquad v = \varepsilon^{-1/2}\nu\,. \tag{1.2}$$

In terms of the new variables $\mathcal{A}$ and ν, (1.1) is transformed to

$$\nu_t = \varepsilon^2 \nu_{xx} - \nu + \mathcal{A}u\nu^2\,, \quad -1 < x < 1\,, \quad t > 0\,; \quad \nu_x(\pm 1, t) = 0\,, \tag{1.3a}$$

$$\tau u_t = Du_{xx} + (1-u) - \varepsilon^{-1}u\nu^2 \quad -1 < x < 1\,, \quad t > 0\,; \quad u_x(\pm 1, t) = 0\,. \tag{1.3b}$$

The semi-strong interaction regime corresponds to $\varepsilon^2 \ll 1$ and $D = O(1)$. The weak-interaction regime, where both components localize, corresponds to the parameter range $D = O(\varepsilon^2) \ll 1$.

The numerical study of [35] for the GS model in the weak-interaction regime in a two-dimensional domain showed a plethora of spike-type patterns in many different parameter ranges, including: time-dependent oscillating spikes; spike death due to over-crowding effects; spike-replication behavior; spatio-temporal chaos; labyrinthian patterns and zigzag instabilities, etc. Many of these behaviors have been qualitatively reproduced in certain chemical experiments (cf. [22], [23]). These studies have stimulated much theoretical work to classify spike behavior in one spatial dimension, including: spike-replication and dynamics in the weak-interaction regime (cf. [36], [37], [38], [31], [41]); spatio-temporal chaos in the weak-interaction regime (cf. [32], [34]; the existence and stability of equilibrium spike patterns in the semi-strong interaction regime (cf. [7], [4], [5], [26], [27], [28], [17], [18]); the dynamics of slowly

modulated two-spike solutions in the semi-strong interaction regime (cf. [2], [3]). Despite these advances, much theoretical work is still needed to quantify the various behaviors discovered in [35].

There has been a largely parallel theoretical analysis of spike-type patterns for the Gierer-Meinhardt (GM) model of [13] used to model various problems in biological morphogenesis, including sea-shell patterns (cf. [25]). The basic GM model can be written in dimensionless form as (cf. [42])

$$a_t = \varepsilon^2 a_{xx} - a + \frac{a^p}{h^q}\,, \quad -1 < x < 1\,, \quad t > 0\,; \qquad a_x(\pm 1, t) = 0\,, \tag{1.4a}$$

$$\tau h_t = D h_{xx} - h + \varepsilon^{-1}\frac{a^m}{h^s}\,, \quad -1 < x < 1\,, \quad t > 0\,; \qquad h_x(\pm 1, t) = 0\,. \tag{1.4b}$$

Here $\varepsilon \ll 1$, $D > 0$, and $\tau \geq 0$, are constants, and the exponent set (p, q, m, s) satisfies (cf. [13]):

$$p > 1\,, \qquad q > 0\,, \qquad m > 1\,, \qquad s \geq 0\,, \qquad \text{with} \qquad \zeta \equiv \frac{qm}{(p-1)} - (s+1) > 0\,. \tag{1.5}$$

Motivated largely by the review article [30], there are now many results for spike-type patterns of the GM model (1.4) in one spatial dimension, including: the existence and stability of equilibrium spike patterns in the semi-strong regime (cf. [44], [16], [6], [42], [43]); the dynamics of spike patterns in the semi-strong interaction regime in various limiting cases (cf. [15], [39], [9]); spike-replication behavior in the weak-interaction regime where $D = O(\varepsilon^2)$ (cf. [33], [8], [20]).

Our main goal is to show that the GS model (1.3) in the low-feed rate regime and the GM model (1.4) have a remarkable similarity with respect to both the dynamics of spikes and to the mechanisms through which quasi-equilibrium spike patterns are de-stabilized. In order to give a precise analytical comparison between the solution behavior for the two models, we focus only on the dynamical behavior of one-spike and symmetric two-spike solutions to (1.3) and (1.4).

In §2 a formal asymptotic method is used to derive ODE's for the time-dependent locations of the spikes for one-spike and two-spike symmetric solutions to the GS model (1.3) and the GM model (1.4). The spikes are shown to move slowly, with a speed $O(\varepsilon^2) \ll 1$. For both models, in §2 we derive nonlocal eigenvalue problems (NLEP) that determine the stability of the spike pattern on a fast $O(1)$ time-scale. Each NLEP depends on D, on τ, and on the spike locations at a given time. From a detailed spectral analysis, in §3 it is shown that eigenvalues can enter the unstable right half-plane along either the real axis or through a Hopf bifurcation, leading to either a competition instability or an oscillatory instability of the spike pattern, respectively. Competition instabilities occur only for two-spike solutions, and not for one-spike solutions, and numerically we show that they lead to the annihilation of one of the two spikes. Oscillatory instabilities occur for both one and two-spike solutions. For two-spike solutions this instability is shown to synchronize the amplitudes of the two spikes. The Propositions given in §3 are rigorous spectral results. In §4 we compare our theoretical results with full numerical computations.

Since the nonlocal eigenvalue problems depend on the instantaneous spike locations, the key feature of these instabilities are that they can be dynamic in nature, and so can be triggered during the slow evolution of a spike pattern. More specifically, our analysis has revealed the phenomena of dynamic instabilities, whereby slowly traveling spikes, that are initially stable on an $O(1)$ time-scale at $t = 0$,

eventually experience the onset of a sudden competition or oscillatory instability as a result of the spikes entering an unstable zone at some point during their evolution towards an equilibrium configuration. We refer to this type of instability as either a *dynamic* competition instability or a *dynamic* oscillatory instability depending on whether the instability leads to the annihilation of spikes or triggers spike oscillations, respectively. This dynamic phenomenon is distinct from a static competition or oscillatory instability that occurs immediately at $t = 0$ when the spike locations are initially in the unstable zone. Our stability analysis for the finite-domain problem gives a quantitative and precise theoretical understanding for the qualitative notion that spikes that are initially stable at $t = 0$ can be destabilized at later times as a result of their mutual interaction or from their interaction with the boundary.

A rough sketch of the nature of these instabilities is as follows. For a fixed small value of τ, a competition instability occurs when either D is too large, or when the spikes are too close together or too close to the boundary of the domain. For D large, the inhibitor (h or u) diffuses over a large spatial extent thereby preventing the occurrence of another spike. The instability for closely spaced spikes is probably a counterpart of the spike over-crowding instability observed numerically in the weak-interaction regime in [35]. Alternatively, for a fixed D, oscillatory instabilities occur when τ is sufficiently large. For τ large, the inhibitor field responds sluggishly to small temporal changes in the spike pattern. This leads to an oscillatory feedback loop typical in delay-type differential equations.

Although there is a direct equivalence between spike behavior in (1.3) and (1.4), the GS model (1.1) in the high feed-rate regime has even richer spike phenomena. For $A = O(1)$, pulse-splitting behavior occurs (cf. [4], [28], [18]), and a traveling wave-type instability occurs when $\tau = O(\varepsilon^{-1})$ (cf. [26], [18]). The stability and asymptotic construction of equilibrium solutions in this regime is given in [28] and [18]. The slow propagation of spikes for the GS model in the pulse-splitting regime $A = O(1)$ is studied in [37] and [38]. The GS model (1.1) in the intermediate regime, defined by $O(\varepsilon^{1/2}) \ll A \ll O(1)$ for $D = O(1)$, provides a bridge between the low feed-rate regime $A = O(\varepsilon^{1/2})$ and the pulse-splitting regime $A = O(1)$. This intermediate regime has no counterpart in the GM model.

Previous related work on a bounded domain is the stability analyses of [17] and [42] of k-spike equilibria to the GS model (1.3) and the GM model (1.4). However, in the context of quasi-equilibrium solutions, the nonlocal eigenvalue problems in Principal Results 2.1–2.3 are new formal asymptotic results and have not appeared previously. In addition, Principal Results 2.1–2.2 characterizing the dynamics of one and two-spike patterns for the GS model (1.3) are new formal asymptotic results, although the derivation is somewhat similar to that given in [15] for the GM model (1.4). Principal Result 2.3 for a two-spike quasi-equilibrium solution to the GM model (1.4) formally extends the analysis in [15] to the case $\tau > 0$ where spike oscillations can occur. The first observation of a dynamic oscillatory instability was given in [39] for a one-spike solution of the GM model. Principal Result 2.4 below, obtained by formal asymptotics, is quoted directly from [39].

Our study on a bounded domain is complementary to the study of certain infinite-domain problems given in [2], [3], and [9]. In [2] and [3], the asymptotic construction of two-spike quasi-equilibria and their stability was analyzed in several distinct parameter regimes using an alternative dimensionless

form of the GS model. By taking the limit $D \to 0$ in our results for the finite-domain problem, in §5.1 we obtain some new results for instability thresholds for static competition and oscillatory instabilities for the infinite-line GS and GM models. For the GS model in the intermediate regime, it is shown in Appendix A that our results for a static oscillatory instability agree with those found earlier in [2] and [3]. Although both static and dynamic instabilities are found to occur for the finite-domain problem, we show that only static instabilities can occur for the infinite-line problem. For the infinite-line problem, it was shown in [2], [4], [6], and [9], that there is an equivalence principle regarding the dynamics and stability of spike patterns in certain parameter ranges of the GM and GS models in the semi-strong interaction limit. In §5.2 we discuss the relationship between that equivalence principle and our equivalence principle for the finite domain problem. Finally, in §6 we conclude with a brief discussion and a short list of some open problems.

2 Spike Dynamics and Nonlocal Eigenvalue Problems

For $\varepsilon \to 0$, we use the method of matched asymptotic expansions to determine the dynamics of symmetric two-spike quasi-equilibrium solutions to the GS model (1.3) in the low-feed rate regime. We also derive a nonlocal eigenvalue problem that determines the stability of such solutions on an $O(1)$ time-scale. We first derive equations of motion for the locations $x_1 = -x_0$ of the two spikes. In each inner region near $x = x_j$, for $j = 0, 1$, we introduce the local variables $\nu_j(y) = \nu(x_j + \varepsilon y)$ and $u_j(y) = u(x_j + \varepsilon y)$, and we expand

$$\nu_j = \nu_{j0}(y,\sigma) + \varepsilon\nu_{j1}(y,\sigma) + \dots\,, \quad u_j = u_{j0}(y,\sigma) + \varepsilon u_{j1}(y,\sigma) + \dots\,, \quad y = \varepsilon^{-1}\left[x - x_j(\sigma)\right]\,, \quad \sigma = \varepsilon^2 t\,. \tag{2.1}$$

We assume that $O(\varepsilon) \ll x_1 \ll 1 - O(\varepsilon)$ so that the spikes are not $O(\varepsilon)$ close to each other or to the boundary. Substituting (2.1) into (1.3), we get that the solution to the leading-order inner problem is

$$u_{j0} = U_j\,, \qquad \nu_{j0} = \frac{1}{\mathcal{A}U_j} w(y)\,. \tag{2.2}$$

Here $U_j = U_j(\sigma)$ are functions to be found, and $w(y) = \frac{3}{2}\mathrm{sech}^2(y/2)$ is the homoclinic solution to

$$w'' - w + w^2 = 0\,, \quad -\infty < y < \infty\,; \quad w \to 0 \quad \text{as} \quad |y| \to \infty\,; \quad w'(0) = 0\,, \quad w(0) > 0\,. \tag{2.3}$$

At the next order we get

$$L\nu_{j1} \equiv \nu_{j1}'' - \nu_{j1} + 2\mathcal{A}u_{j0}\nu_{j0}\nu_{j1} = -\mathcal{A}u_{j1}\nu_{j0}^2 - \frac{dx_j}{d\sigma}\nu_{j0}'\,; \qquad Du_{j1}'' = u_{j0}\nu_{j0}^2\,, \tag{2.4}$$

on $-\infty < y < \infty$, with $\nu_{j1} \to 0$ exponentially as $|y| \to \infty$. To determine $dx_j/d\sigma$, we use a solvability condition that $L\nu_{j1}$ must be orthogonal to w'. Upon integrating this solvability condition by parts twice, and using $\int_{-\infty}^{\infty} w^3\,dy = 6\int_{-\infty}^{\infty} w'^2\,dy$ from (2.3), we can readily show that

$$\frac{dx_j}{d\sigma} = \frac{1}{U_j}\left[u_{j1}'(+\infty) + u_{j1}'(-\infty)\right]\,. \tag{2.5}$$

Next, we consider the outer problem for $u = u(x, \sigma)$, which is valid away from $O(\varepsilon)$ regions centered at $x = x_j$ for $j = 0, 1$. The matching of this solution to the inner solution determines both U_j and $u_{j1}'(\pm\infty)$. Since $\varepsilon^{-1} u\nu^2$ is localized near each $x = x_j$, its effect in the outer region can be calculated in the sense of distributions. From (2.2), and $\int_{-\infty}^{\infty} w^2\, dy = 6$, we obtain that

$$Du_{xx} + 1 - u = \sum_{i=0}^{1} \frac{6}{\mathcal{A}^2 U_i} \delta(x - x_i)\,, \qquad -1 < x < 1\,; \qquad u_x(\pm 1) = 0\,. \tag{2.6}$$

The solution to (2.6) is

$$u = 1 - \sum_{i=0}^{1} \frac{6}{\mathcal{A}^2 U_i} G_0(x; x_i)\,, \tag{2.7}$$

where $G_0(x; x_i)$ is the Green's function satisfying

$$DG_{0xx} - G_0 = -\delta(x - x_0)\,, \quad -1 < x < 1\,; \qquad G_{0x}(\pm 1; x_0) = 0\,. \tag{2.8}$$

The first matching condition is that $u(x_j) = U_j$ for $j = 0, 1$. Since we are seeking symmetric solutions, we have from (2.7) that the common value $U_j = U$ for $j = 0, 1$, is

$$U = 1 - \frac{6 a_g}{\mathcal{A}^2 U}\,, \qquad a_g \equiv G_0(x_0; x_0) + G_0(x_0; x_1)\,. \tag{2.9}$$

For $\mathcal{A} > \mathcal{A}_{2e}$, this quadratic equation for U has two roots

$$U_{\pm} = \frac{1}{2}\left[1 \pm \sqrt{1 - \left(\frac{\mathcal{A}_{2e}}{\mathcal{A}}\right)^2}\right]\,, \qquad \mathcal{A}_{2e} \equiv \sqrt{24 a_g}\,. \tag{2.10}$$

It is convenient below to note that a_g is an eigenvalue of the Green's function matrix $\mathcal{G}_0$ defined by

$$\mathcal{G}_0 \boldsymbol{e} = a_g \boldsymbol{e}\,, \qquad \mathcal{G}_0 \equiv \begin{pmatrix} G_0(x_0; x_0) & G_0(x_0; x_1) \\ G_0(x_1; x_0) & G_0(x_1; x_1) \end{pmatrix}\,, \qquad \boldsymbol{e} \equiv \begin{pmatrix} 1 \\ 1 \end{pmatrix}\,. \tag{2.11}$$

The other matching conditions are that $u_x(x_j^{\pm}) = u_{j1}'(\pm\infty)$ for $j = 0, 1$. This yields

$$u_{01}'(\pm\infty) = -\frac{s_g U}{a_g}\left(G_{0x}(x_0^{\pm}; x_0) + G_{0x}(x_0; x_1)\right)\,, \quad u_{11}'(\pm\infty) = -\frac{s_g U}{a_g}\left(G_{0x}(x_1^{\pm}; x_1) + G_{0x}(x_1; x_0)\right)\,. \tag{2.12}$$

In obtaining (2.12), we have re-written (2.9) in the form

$$\frac{6}{\mathcal{A}^2 U^2} = \frac{s_g}{a_g}\,, \qquad s_g \equiv \frac{1 - U}{U}\,. \tag{2.13}$$

Substituting (2.12) into (2.5), we write the differential equations for x_0, x_1 in matrix form as

$$\frac{d\boldsymbol{x}}{d\sigma} = -\frac{2 s_g}{a_g} \mathcal{P}_0 \boldsymbol{e}\,, \qquad \boldsymbol{x} \equiv \begin{pmatrix} x_0 \\ x_1 \end{pmatrix}\,, \tag{2.14}$$

where the matrix $\mathcal{P}_0$ is defined by

$$\mathcal{P}_0 \equiv \begin{pmatrix} \langle G_{0x}\rangle_0 & G_{0x}(x_0;x_1) \\ G_{0x}(x_1;x_0) & \langle G_{0x}\rangle_1 \end{pmatrix}, \qquad \langle G_{0x}\rangle_j \equiv \frac{1}{2}\left[G_{0x}(x_j^+;x_j) + G_{0x}(x_j^-;x_j)\right]. \tag{2.15}$$

A direct calculation of (2.11) and (2.14) in terms of the Green's function leads to seemingly very complicated expressions for a_g and for the dynamical law for $\boldsymbol{x}$. To circumvent this difficulty we use some matrix identities, as proved in Appendix A of [15], that show that the inverses of $\mathcal{G}_0$ and $\mathcal{P}_0$ can be easily expressed in terms of x_0 and x_1 by two additional matrices $\mathcal{P}_{b0}$ and $\mathcal{B}_0$ as

$$\mathcal{P}_0 \equiv \frac{1}{2D}\mathcal{P}_{b0}\mathcal{B}_0^{-1}, \qquad \mathcal{G}_0 \equiv \frac{1}{\sqrt{D}}\mathcal{B}_0^{-1}, \qquad \mathcal{B}_0 \equiv \begin{pmatrix} c_1 & d_1 \\ d_1 & c_1 \end{pmatrix}, \qquad \mathcal{P}_{b0} \equiv \begin{pmatrix} e_1 & f_1 \\ -f_1 & -e_1 \end{pmatrix}. \tag{2.16}$$

For $x_1 = -x_0$, the matrix entries are given in terms of $\theta_0 = D^{-1/2}$ by

$$c_1 = \coth(\theta_0(x_1 - x_0)) + \tanh(\theta_0(1 + x_0)), \qquad d_1 = -\operatorname{csch}(\theta_0(x_1 - x_0)), \tag{2.17a}$$

$$e_1 = -\coth(\theta_0(x_1 - x_0)) + \tanh(\theta_0(1 + x_0)), \qquad f_1 = \operatorname{csch}(\theta_0(x_1 - x_0)). \tag{2.17b}$$

Substituting the formula for $\mathcal{G}_0$ from (2.16) into (2.11), we get that a_g satisfies

$$a_g\sqrt{D}\,\mathcal{B}_0\boldsymbol{e} = \boldsymbol{e}, \qquad a_g\sqrt{D} = [c_1 + d_1]^{-1}. \tag{2.18}$$

By substituting (2.18) into (2.14), and using (2.16) for $\mathcal{P}_0\mathcal{B}_0$, we obtain the dynamical law

$$\frac{dx_0}{d\sigma} = -\frac{s_g}{\sqrt{D}}(e_1 + f_1), \qquad \frac{dx_1}{d\sigma} = \frac{s_g}{\sqrt{D}}(e_1 + f_1). \tag{2.19}$$

Substituting the expressions for e_1 and f_1 from (2.17b) into (2.19), we obtain explicit differential equations for x_0 and x_1. The result is given below in Principal Result 2.1.

Next, we derive a nonlocal eigenvalue problem that determines the stability of a two-spike quasi-equilibrium solution for the GS model (1.3) in the low feed-rate regime for $x_1 = -x_0$ fixed. Let u_e, ν_e denote the two-spike quasi-equilibrium solution, and set $\nu = \nu_e + e^{\lambda t}\phi$ and $u = u_e + e^{\lambda t}\eta$, where $\phi \ll 1$ and $\eta \ll 1$. Substituting this into (1.3), and linearizing, we obtain the eigenvalue problem

$$\varepsilon^2\phi_{xx} - \phi + 2\mathcal{A}u_e\nu_e\phi + \mathcal{A}\eta\nu_e^2 = \lambda\phi, \quad -1 < x < 1; \qquad \phi_x(\pm 1) = 0, \tag{2.20a}$$

$$D\eta_{xx} - \eta - \varepsilon^{-1}\nu_e^2\eta - 2\varepsilon^{-1}u_e\nu_e\phi = \tau\lambda\eta, \quad -1 < x < 1; \qquad \eta_x(\pm 1) = 0. \tag{2.20b}$$

We look for eigenvalues of (2.20) that are $O(1)$ as $\varepsilon \to 0$. The corresponding eigenfunction has the form

$$\phi(x) \sim \sum_{i=0}^{1} \phi_i\left[\varepsilon^{-1}(x - x_i)\right], \tag{2.21}$$

where $\phi_i(y) \to 0$ exponentially as $|y| \to \infty$. Since ν_e and ϕ are localized when $\varepsilon \ll 1$, we obtain in the sense of distributions that near each x_j

$$\varepsilon^{-1}\nu_e^2 \sim \frac{6}{\mathcal{A}^2U^2}\delta(x - x_j); \qquad 2\varepsilon^{-1}u_e\nu_e\Phi \sim \frac{2}{\mathcal{A}}\left(\int_{-\infty}^{\infty} w\Phi\,dy\right)\delta(x - x_j). \tag{2.22}$$

Upon substituting (2.22) into (2.20b), we obtain that η satisfies

$$D\eta_{xx} - (1+\tau\lambda)\eta = 0\,, \quad -1 < x < 1\,; \qquad \eta_x(\pm 1) = 0\,, \tag{2.23a}$$

$$[\eta]_j = 0\,, \qquad [D\eta_x]_j = -\omega_j + \frac{6\eta(x_j)}{\mathcal{A}^2U^2}\,, \quad h = 0,1\,; \qquad \omega_j \equiv -\frac{2}{\mathcal{A}}\int_{-\infty}^{\infty} w\phi_j\,dy\,. \tag{2.23b}$$

Substituting (2.21) into (2.20a), and using $\nu_e \sim (\mathcal{A}U)^{-1}\,w$ and $u_e \sim U$ in the core of each spike, we obtain that ϕ_j satisfies

$$\phi_j'' - \phi_j + 2w\phi_j + \frac{\eta(x_j)}{\mathcal{A}U^2}w^2 = \lambda\phi_j\,, \qquad -\infty < y < \infty\,. \tag{2.24}$$

Next, we solve (2.23) for $\eta(x)$ to get

$$\eta(x) = \sum_{i=0}^{1} G_\lambda(x;x_i)\omega_i - \frac{6}{\mathcal{A}^2U^2}\sum_{i=0}^{1} G_\lambda(x;x_i)\eta(x_i)\,. \tag{2.25}$$

Here $G_\lambda(x;x_j)$ is the Green's function that satisfies

$$DG_{\lambda xx} - (1+\tau\lambda)G_\lambda = -\delta(x-x_j)\,, \quad -1 < x < 1\,; \qquad G_{\lambda x}(\pm 1;x_j) = 0\,. \tag{2.26}$$

Defining $\boldsymbol{\eta} \equiv (\eta(x_0),\eta(x_1))^t$, we use (2.25) to write $\boldsymbol{\eta}$ in matrix form as

$$\left(\frac{6}{\mathcal{A}^2U^2}\mathcal{G}_\lambda + I\right)\boldsymbol{\eta} = \mathcal{G}_\lambda\boldsymbol{\omega}\,, \tag{2.27a}$$

where $\mathcal{G}_\lambda$ and $\boldsymbol{\omega}$ are defined by

$$\mathcal{G}_\lambda \equiv \begin{pmatrix} G_\lambda(x_0;x_0) & G_\lambda(x_0;x_1) \\ G_\lambda(x_1;x_0) & G_\lambda(x_1;x_1) \end{pmatrix}\,, \qquad \boldsymbol{\omega} \equiv \begin{pmatrix} \omega_0 \\ \omega_1 \end{pmatrix}\,. \tag{2.27b}$$

We then calculate that

$$\mathcal{G}_\lambda \equiv \frac{1}{D\theta_\lambda}\mathcal{B}_\lambda^{-1}\,, \qquad \theta_\lambda \equiv \theta_0\sqrt{1+\tau\lambda}\,, \qquad \theta_0 \equiv D^{-1/2}\,. \tag{2.28}$$

Here $\mathcal{B}_\lambda$ is the matrix

$$\mathcal{B}_\lambda \equiv \begin{pmatrix} c_\lambda & d_\lambda \\ d_\lambda & c_\lambda \end{pmatrix}\,, \tag{2.29}$$

where the matrix entries, with $x_1 = -x_0$, are given by

$$c_\lambda = \coth(\theta_\lambda(x_1-x_0)) + \tanh(\theta_\lambda(1+x_0))\,, \qquad d_\lambda = -\mathrm{csch}(\theta_\lambda(x_1-x_0))\,. \tag{2.30}$$

Substituting (2.28) into (2.27a), and using (2.13), we obtain that

$$\boldsymbol{\eta} = \frac{1}{D\theta_\lambda}\left(\mathcal{B}_\lambda + \frac{s_g}{a_g D\theta_\lambda}I\right)^{-1}\boldsymbol{\omega}\,. \tag{2.31}$$

Substituting (2.31) into (2.24), and using (2.23b) for ω_j, we get the nonlocal eigenvalue problem

$$\boldsymbol{\phi}'' - \boldsymbol{\phi} + 2w\boldsymbol{\phi} - \frac{12w^2}{\mathcal{A}^2U^2D\theta_\lambda}\left(\mathcal{B}_\lambda + \frac{s_g}{a_gD\theta_\lambda}I\right)^{-1}\left(\frac{\int_{-\infty}^{\infty} w\boldsymbol{\phi}\,dy}{\int_{-\infty}^{\infty} w^2\,dy}\right) = \lambda\boldsymbol{\phi}\,. \tag{2.32}$$

Here $\boldsymbol{\phi} \equiv (\phi_0, \phi_1)^t$. To diagonalize (2.32) we calculate the spectrum of $\mathcal{B}_\lambda$ as

$$\mathcal{B}_\lambda \boldsymbol{c} = \kappa \boldsymbol{c}\,, \qquad \kappa_\pm \equiv c_\lambda \pm d_\lambda\,, \qquad \boldsymbol{c}_\pm = (1, \pm 1)^t\,. \tag{2.33}$$

Here c_λ and d_λ are given in (2.30). It then follows that $\boldsymbol{\phi} = \boldsymbol{c}\Phi$, for some scalar function $\Phi(y)$. Furthermore, it follows from the definition of a_g in (2.18) that $a_g\sqrt{D} = 1/\kappa_+$ when $\lambda = 0$.

Equation (2.33) shows that $\kappa_\pm = \kappa_\pm(\tau\lambda)$. In the analysis below, we require an explicit formula for $\kappa_\pm(\tau\lambda)/\kappa_+(0)$. Using (2.33) and (2.30), we calculate that

$$\frac{\kappa_+(\tau\lambda)}{\kappa_+(0)} = \frac{\tanh(\theta_\lambda\alpha) + \tanh(\theta_\lambda(1-\alpha))}{\tanh(\theta_0\alpha) + \tanh(\theta_0(1-\alpha))}\,, \qquad \frac{\kappa_-(\tau\lambda)}{\kappa_+(0)} = \frac{\coth(\theta_\lambda\alpha) + \tanh(\theta_\lambda(1-\alpha))}{\tanh(\theta_0\alpha) + \tanh(\theta_0(1-\alpha))}\,, \tag{2.34}$$

where $\alpha \equiv x_1 = -x_0$. Substituting (2.33) into (2.32) we get the nonlocal eigenvalue problem (NLEP).

For the GS model (1.3), we summarize the derivation of the dynamics of two-spike quasi-equilibria, and of the NLEP governing its stability on an $O(1)$ time-scale, in the following main result:

Principal Result 2.1: *Consider a symmetric quasi-equilibrium two-spike solution for the GS model (1.3) where the spikes are located at $\alpha \equiv x_1 = -x_0 > 0$, with $\alpha \gg O(\varepsilon)$ and $1-\alpha \gg O(\varepsilon)$. Suppose that $\mathcal{A} > \mathcal{A}_{2e}$, where $\mathcal{A}_{2e} = \mathcal{A}_{2e}(\alpha)$ is the existence threshold defined in (2.10), and given explicitly by*

$$\mathcal{A}_{2e} = \frac{\sqrt{24\theta_0}}{\left(\tanh[\theta_0\alpha] + \tanh[\theta_0(1-\alpha)]\right)^{1/2}} = \sqrt{\frac{12\theta_0}{\sinh\theta_0}}\left(\cosh\theta_0 + \cosh\left[2\theta_0\left(\alpha - 1/2\right)\right]\right)^{1/2}\,, \quad \theta_0 \equiv D^{-1/2}\,. \tag{2.35}$$

Then, for $0 < \varepsilon \ll 1$ and $\tau = 0(1)$, and assuming that the quasi-equilibrium solution is stable on an $O(1)$ time scale, the dynamics of such a solution with $\sigma = \varepsilon^2 t$ is given by

$$\nu(x,\sigma) \sim \nu_e \equiv \frac{1}{\mathcal{A}U}\left[w\left(\varepsilon^{-1}[x - x_0(\sigma)]\right) + w\left(\varepsilon^{-1}[x - x_1(\sigma)]\right)\right]\,, \tag{2.36a}$$

$$u(x,\sigma) \sim u_e \equiv 1 - \frac{(1-U)}{a_g}\sum_{i=0}^{1} G_0(x;x_i)\,, \quad |x - x_i| \gg O(\varepsilon)\,, \quad i = 0, 1\,, \tag{2.36b}$$

where the spike locations $\alpha \equiv x_1 = -x_0$ satisfy the ODE

$$\frac{d\alpha}{dt} \sim \varepsilon^2\theta_0 s_g\left[\tanh(\theta_0(1-\alpha)) - \tanh(\theta_0\alpha)\right]\,, \qquad \theta_0 = D^{-1/2}\,. \tag{2.36c}$$

Here $w(y)$, a_g, G_0, and U, satisfy (2.3), (2.18), (2.8), and (2.10). In (2.36c), s_g defined in (2.13) depends on α, and can be written explicitly in terms of $\mathcal{A}$ and $\mathcal{A}_{2e}$ as

$$s_g = 2\left[1 \pm \sqrt{1 - \left(\frac{\mathcal{A}_{2e}}{\mathcal{A}}\right)^2}\right]^{-1} - 1\,. \tag{2.36d}$$

The stability of ν_e and u_e on an $O(1)$ time-scale is determined by the spectrum of the NLEP

$$L_0\Phi - \chi_{gs\pm} w^2 \left(\frac{\int_{-\infty}^{\infty} w\Phi\, dy}{\int_{-\infty}^{\infty} w^2\, dy} \right) = \lambda\Phi\,, \quad -\infty < y < \infty\,; \quad \Phi \to 0 \quad \text{as} \quad |y| \to \infty\,. \tag{2.37a}$$

In (2.37a), the local operator L_0 is $L_0\Phi = \Phi'' - \Phi + 2w\Phi$, and the multiplier $\chi_{gs\pm}$ is defined by

$$\chi_{gs\pm} \equiv 2s_g \left[s_g + \sqrt{1+\tau\lambda} \left(\frac{\kappa_\pm(\tau\lambda)}{\kappa_+(0)} \right) \right]^{-1}\,. \tag{2.37b}$$

Here $\kappa_\pm(\tau\lambda)/\kappa_+(0)$ are defined in (2.34). The corresponding localized eigenfunction has the form

$$\phi(x) = \sum_{i=0}^{1} \Phi(\varepsilon^{-1}(x - x_i)) \quad \text{for} \quad \chi_{gs+}\,; \qquad \phi(x) = \sum_{i=0}^{1} (-1)^i \Phi(\varepsilon^{-1}(x - x_i)) \quad \text{for} \quad \chi_{gs-}\,. \tag{2.37c}$$

For the equilibrium problem, an analogous NLEP was derived in Proposition 3.2 of [17] for the stability of k-spike equilibria in the GS model (1.3). However, in the context of quasi-equilibrium solutions, the NLEP (2.37), the existence threshold $\mathcal{A}_{2e} = \mathcal{A}_{2e}(\alpha)$, and the dynamics (2.36c), are new results and have not appeared in the literature. For a one-spike quasi-equilibrium solution for (1.3), the following analogous result, which has not appeared in the literature, can be derived using the method of matched asymptotic expansions. We leave the details to the reader.

Principal Result 2.2: *Consider a quasi-equilibrium one-spike solution for the GS model (1.3), where the spike location $x_0 \in (-1,1)$ satisfies $|x_0+1| \gg O(\varepsilon)$ and $|1-x_0| \gg O(\varepsilon)$. Suppose that $\mathcal{A} > \mathcal{A}_{1e}(x_0)$, where the existence threshold is given explicitly by*

$$\mathcal{A}_{1e} = \frac{\sqrt{24\theta_0}}{\left(\tanh[\theta_0(1-x_0)] + \tanh[\theta_0(1+x_0)]\right)^{1/2}}\,, \qquad \theta_0 \equiv D^{-1/2}\,. \tag{2.38}$$

Then, for $0 < \varepsilon \ll 1$ and $\tau = 0(1)$, and assuming that the quasi-equilibrium solution is stable on an $O(1)$ time scale, the dynamics of such a solution with $\sigma = \varepsilon^2 t$ is given by

$$\nu(x,\sigma) \sim \nu_e \equiv \frac{1}{\mathcal{A}U} w\left(\varepsilon^{-1}[x - x_0(\sigma)]\right)\,; \quad u(x,\sigma) \sim u_e \equiv 1 - (1-U)\frac{G_0(x;x_0)}{G_0(x_0;x_0)}\,, \quad |x - x_0| \gg O(\varepsilon)\,, \tag{2.39a}$$

where the spike location x_0 satisfies the ODE

$$\frac{dx_0}{dt} \sim -\varepsilon^2 \theta_0 s_g \left(\tanh[\theta_0(1+x_0)] - \tanh[\theta_0(1-x_0)]\right)\,, \qquad \theta_0 \equiv D^{-1/2}\,. \tag{2.39b}$$

Here $w(y)$ and G_0 satisfy (2.3) and (2.8). In addition, s_g and U are defined by

$$U_\pm = \frac{1}{2}\left[1 \pm \sqrt{1 - \left(\frac{\mathcal{A}_{1e}}{\mathcal{A}}\right)^2}\right]\,, \qquad s_g = 2\left[1 \pm \sqrt{1 - \left(\frac{\mathcal{A}_{1e}}{\mathcal{A}}\right)^2}\right]^{-1} - 1\,. \tag{2.39c}$$

The stability of ν_e and u_e on an $O(1)$ time-scale is determined by the spectrum of the NLEP (2.37a) where $\chi_{gs\pm}$ in (2.37a) is replaced with χ_{gs}, where

$$\chi_{gs} \equiv 2s_g \left[s_g + \sqrt{1+\tau\lambda} \left(\frac{\beta(\theta_\lambda; x_0)}{\beta(\theta_0; x_0)} \right) \right]^{-1}, \quad \beta(\xi; x_0) \equiv \tanh[\xi(1+x_0)] + \tanh[\xi(1-x_0)]\,. \tag{2.40}$$

Here $\theta_\lambda \equiv \theta_0\sqrt{1+\tau\lambda}$ and $\theta_0 \equiv D^{-1/2}$.

In Fig. 1(a) we plot the existence threshold $\mathcal{A}_{1e}$, defined in (2.38), as a function of x_0 for three values of D. It is readily shown that $\mathcal{A}_{1e}$ has its minimum value at $x_0 = 0$ for any $D > 0$. Therefore, the minimum value of $\mathcal{A}$ for which a quasi-equilibrium solution exists occurs when the spike is at the origin. In Fig. 1(b) we plot the quasi-equilibrium solution for $\nu(x)$ for two values of x_0, where we have taken the minus root for U in (2.39c). As a partial check on the analysis, notice that $\mathcal{A}_{1e}$ at $x_0 = 0$ and with θ_0 replaced by $2\theta_0$ is the same as $\mathcal{A}_{1e}$ at $x_0 = 1$. This equivalence results from the fact that $\mathcal{A}_{1e}$ at $x_0 = 1$ corresponds to an interior spike solution on a domain of twice the original length. Therefore, this threshold must be the same as decreasing D for the problem on $-1 < x < 1$ by a factor of four.

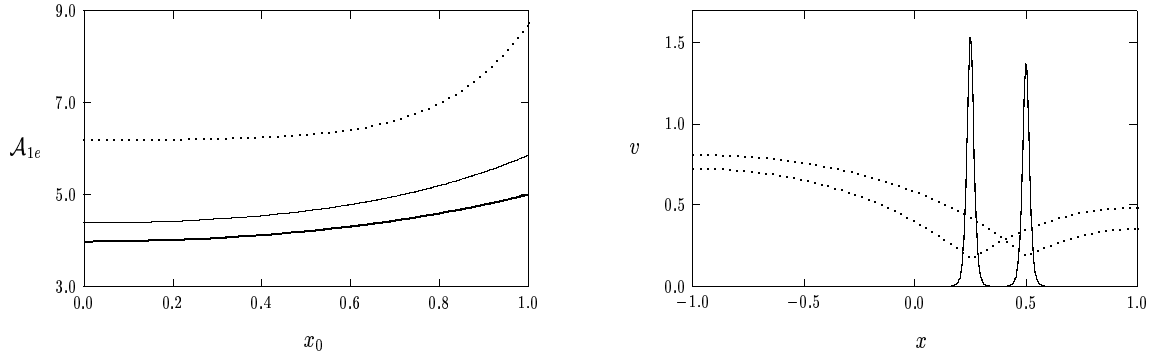

(a) $\mathcal{A}_{1e}$ versus x_1

(b) ν_e and u_e versus x

Figure 1: Left figure: $\mathcal{A}_{1e}$ versus x_0, given in (2.38), for $D = 1.0$ (heavy solid curve), $D = 0.5$ (solid curve), and $D = 0.1$ (dotted curve). Right figure: Plot of quasi-equilibrium solution ν_e (solid curve) and u_e (dotted curve) for $x_0 = 0.25$ and $x_0 = 0.5$ when $\mathcal{A} = 6.0$, $D = 0.5$, and $\varepsilon = 0.1$.

In Fig. 2(a) we plot the existence threshold $\mathcal{A}_{2e}$ for a two-spike solution, defined in (2.35), as a function of $\alpha = x_1$ for three values of D. A simple calculation shows that, for any $D > 0$, $\mathcal{A}_{2e}$ always has its minimum value at $\alpha = 1/2$, which corresponds to the location of the rightmost spike for a two-spike equilibrium solution. This symmetry for $\mathcal{A}_{2e}$ about $\alpha = 1/2$ is clear in that there is an image spike reflected across the boundary $x = 1$ due to the Neumann boundary conditions. Hence, two spikes centered at $-\alpha$ and α with $\alpha < 1/2$ must have the same existence threshold as two spikes centered at $\alpha > 1/2$ and $2 - \alpha$. For $D = 0.1$, in Fig. 2(b) we compare the existence threshold $\mathcal{A}_{1e}$ for a

one-spike quasi-equilibrium solution centered at $\alpha = x_0$ with the existence threshold $\mathcal{A}_{2e}$ of a two-spike quasi-equilibrium solution where the rightmost spike is at $x_1 = \alpha$. It is readily shown using (2.38) and (2.35) that $\mathcal{A}_{2e} > \mathcal{A}_{1e}$ for any $D > 0$ and $\alpha > 0$. Therefore, two-spike quasi-equilibria exist in the range $\mathcal{A}_{1e} < \mathcal{A} < \mathcal{A}_{2e}$ where there is no one-spike quasi-equilibrium solution.

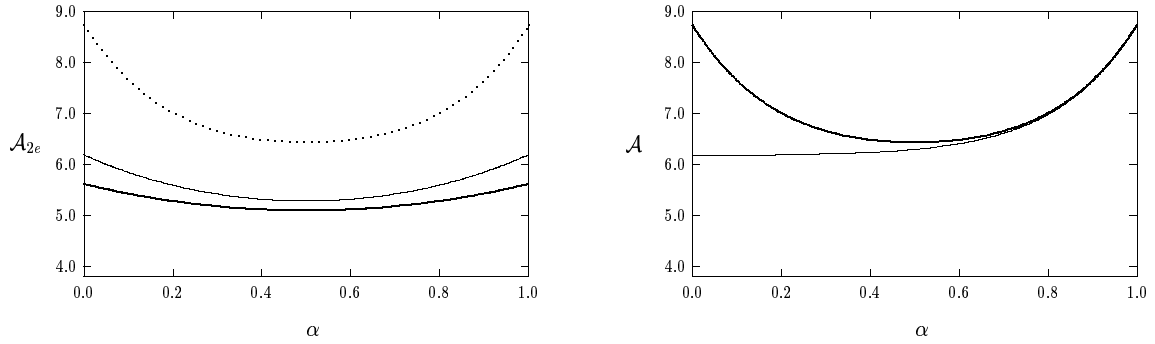

(a) $\mathcal{A}_{2e}$ versus $\alpha = x_1$

(b) $\mathcal{A}_{2e}$ and $\mathcal{A}_{1e}$ versus $\alpha = x_1$

Figure 2: Left figure: $\mathcal{A}_{2e}$ versus $\alpha = x_1$, given in (2.35), for $D = 1.0$ (heavy solid curve), $D = 0.5$ (solid curve), and $D = 0.1$ (dotted curve). Right figure: $\mathcal{A}_{1e}$ (solid curve) and $\mathcal{A}_{2e}$ (heavy solid curve) for a one and two-spike quasi-equilibrium solution, respectively, when $D = 0.1$.

In §3 where we give a detailed analysis of the nonlocal eigenvalue problems for the GS model, it is convenient to introduce a bifurcation diagram of a norm of ν versus $\mathcal{A}$. For a k-spike quasi-equilibrium solution where $k = 1$ or $k = 2$, we define an L_2 norm, $|\nu|_2$, and then use (2.39) and (2.36) to asymptotically calculate the norm as $\varepsilon \to 0$. In this way, we obtain,

$$|\nu|_2 \equiv \left(\varepsilon^{-1}\int_{-\infty}^{\infty}\nu^2\,dy\right)^{1/2} \sim \frac{2\sqrt{6k}}{\mathcal{A}}\left[1 \pm \sqrt{1-\left(\frac{\mathcal{A}_{ke}}{\mathcal{A}}\right)^2}\right]^{-1}, \tag{2.41}$$

where $\mathcal{A}_{1e}$ and $\mathcal{A}_{2e}$ are the existence thresholds defined in (2.38) and (2.35), respectively.

Principal Results 2.1–2.2 show that when the spike profile is stable, the spike dynamics is asymptotically independent of τ for $\tau = O(1)$. In [15] the dynamics and stability of k-spike quasi-equilibrium patterns for the GM model (1.4) were analyzed only for the special value $\tau = 0$. Using a similar analysis to that for the GS model given above, it can be shown that the spike dynamics for the GM model (1.4) found in [15] also hold for $\tau > 0$ provided that the spike profile is stable. In [15], a nonlocal eigenvalue problem for the stability of a k-spike quasi-equilibrium solution for $\tau = 0$ was derived, and the multiplier of the nonlocal term was determined numerically in terms of the eigenvalues of a matrix eigenvalue problem (see Proposition 4.2 of [15]). The result below for the NLEP extends that analysis to the case $\tau \geq 0$, and to the special case of a two-spike symmetric quasi-equilibrium solution where the multiplier of the nonlocal term can be found analytically. The result is as follows:

Principal Result 2.3: *Consider a symmetric quasi-equilibrium two-spike solution for the GM model (1.4) with spikes at $\alpha \equiv x_1 = -x_0 > 0$, where $\alpha \gg O(\varepsilon)$ and $1-\alpha \gg O(\varepsilon)$. Then, for $0 < \varepsilon \ll 1$ and $\tau = O(1)$, and assuming that the quasi-equilibrium solution is stable on an $O(1)$ time scale, the dynamics of such a solution with $\sigma = \varepsilon^2 t$ is given by*

$$a(x,\sigma) \sim a_e \equiv H^\gamma \left[w\left(\varepsilon^{-1}[x - x_0(\sigma)]\right) + w\left(\varepsilon^{-1}[x - x_1(\sigma)]\right)\right] , \tag{2.42a}$$

$$h(x,\sigma) \sim h_e \equiv \frac{H}{a_g} \sum_{i=0}^{1} G_0(x;x_i) , \qquad H^\zeta = \frac{1}{b_m a_g} , \qquad b_m \equiv \int_{-\infty}^{\infty} w^m \, dy . \tag{2.42b}$$

Here $\gamma \equiv q/(p-1)$ and ζ is defined in (1.5). In addition, a_g, and G_0, satisfy (2.18) and (2.8). The profile $w(y) = \left(\frac{p+1}{2}\right)^{1/(p-1)} \left(\cosh\left[\frac{(p-1)y}{2}\right]\right)^{-2/(p-1)}$ is the homoclinic solution to

$$w'' - w + w^p = 0 , \quad -\infty < y < \infty ; \quad w \to 0 \quad \text{as} \quad |y| \to \infty ; \quad w'(0) = 0 , \quad w(0) > 0 . \tag{2.42c}$$

The spike locations $\alpha \equiv x_1 = -x_0$ satisfy the ODE

$$\frac{d\alpha}{dt} \sim \frac{\varepsilon^2 q \theta_0}{(p-1)} \left[\tanh(\theta_0(1-\alpha)) - \tanh(\theta_0 \alpha)\right] , \qquad \theta_0 = D^{-1/2} . \tag{2.42d}$$

The stability of the quasi-equilibrium profile (2.42a) for the GM model (1.4) on an $O(1)$ time-scale is determined by the spectrum of the NLEP

$$L_0 \Phi - \chi_{gm\pm} w^p \left(\frac{\int_{-\infty}^{\infty} w^{m-1} \Phi \, dy}{\int_{-\infty}^{\infty} w^m \, dy} \right) = \lambda \Phi , \quad -\infty < y < \infty ; \quad \Phi \to 0 \quad \text{as} \quad |y| \to \infty , \tag{2.43a}$$

where the local operator is $L_0 \Phi \equiv \Phi'' - \Phi + p w^{p-1} \Phi$, and the multiplier $\chi_{gm\pm}$ is defined by,

$$\chi_{gm\pm} \equiv qm \left[s + \sqrt{1+\tau\lambda} \left(\frac{\kappa_\pm(\tau\lambda)}{\kappa_+(0)} \right) \right]^{-1} . \tag{2.43b}$$

Here $\kappa_\pm(\tau\lambda)/\kappa_+(0)$ is given explicitly in (2.34). The corresponding localized eigenfunction has the form given in (2.37c) with $\chi_{gs\pm}$ replaced by $\chi_{gm\pm}$ in (2.37c).

The ODE (2.42d) is equivalent to that given in equation (5.3) of Corollary 5.2 of [15]. The corresponding result for the dynamics and the stability of a one-spike quasi-equilibrium solution to the GM model (1.4) was given in Propositions 3.1 and 4.1 of [39]. The result is summarized as follows.

Principal Result 2.4: *Consider a quasi-equilibrium one-spike solution for the GM model (1.4), where the spike location x_0 satisfies $|x_0 + 1| \gg O(\varepsilon)$ and $|1 - x_0| \gg O(\varepsilon)$. Then, for $0 < \varepsilon \ll 1$ and $\tau = 0(1)$, and assuming that the quasi-equilibrium profile is stable on an $O(1)$ time-scale, the dynamics of such a solution with $\sigma = \varepsilon^2 t$ is given by*

$$a(x,\sigma) \sim a_e \equiv H^\gamma w\left(\varepsilon^{-1}[x - x_0(\sigma)]\right) ; \quad h(x,\sigma) \sim h_e \equiv H \frac{G_0(x;x_0)}{G_0(x_0;x_0)} , \quad |x - x_0| \gg O(\varepsilon) . \tag{2.44a}$$

Here $\gamma \equiv q/(p-1)$, $H^{\zeta} = [b_m G_0(x_0;x_0)]^{-1}$ *with* $b_m = \int_{-\infty}^{\infty} w^m\,dy$, *and* ζ *is defined in (1.5). The spike location* x_0 *satisfies the ODE*

$$\frac{dx_0}{dt} \sim -\frac{\varepsilon^2 q\theta_0}{(p-1)}\left(\tanh[\theta_0(1+x_0)] - \tanh[\theta_0(1-x_0)]\right), \qquad \theta_0 \equiv D^{-1/2}. \tag{2.44b}$$

The stability of the quasi-equilibrium profile (2.44a) for the GM model on an $O(1)$ *time-scale is determined by the spectrum of the NLEP (2.43), where* $\chi_{gm\pm}$ *is replaced by* χ_{gm}, *where*

$$\chi_{gm} \equiv qm\left[s + \sqrt{1+\tau\lambda}\left(\frac{\beta(\theta_\lambda;x_0)}{\beta(\theta_0;x_0)}\right)\right]^{-1}, \quad \beta(\xi;x_0) \equiv \tanh[\xi(1+x_0)] + \tanh[\xi(1-x_0)]. \tag{2.45}$$

Here $\theta_\lambda \equiv \theta_0\sqrt{1+\tau\lambda}$ *and* $\theta_0 \equiv D^{-1/2}$.

By comparing the expressions for spike dynamics and the nonlocal eigenvalue problems in Principal Results 2.1–2.4, we observe the following equivalence principle between the GS and GM models:

Principal Result 2.5: *In the limit* $\varepsilon \ll 1$, *the nonlocal eigenvalue problems for the stability of a one and a two-spike quasi-equilibrium solution for the GS model in the low feed-rate regime is equivalent to the nonlocal eigenvalue problems for a one and two-spike quasi-equilibrium solution of a GM model with exponent set* $(p,q,m,s) = (2,s_g,2,s_g)$, *where* s_g *is defined in (2.39c) and (2.36d) for a one-spike and two-spike solution, respectively. The dynamics of spikes, as given in Principal Results 2.1–2.4, also share this equivalence principle up to a multiplicative factor in the time scale.*

A related spectral equivalence principle was given in Proposition 3.3 of [17] regarding k-spike equilibria. Principal Result 2.5 shows that this principle also holds for one and two-spike quasi-equilibrium solutions and for the spike dynamics associated with these solutions. The only issue of concern in this equivalence principle is that the usual assumption on the GM exponent set, from (1.5), is that $\zeta = qm/(p-1) - (1+s) > 0$. For the exponent set $(2,s_g,2,s_g)$, we calculate $\zeta = s_g - 1$. Therefore, the upper bifurcation branch of $|\nu|_2$ versus $\mathcal{A}$, which corresponds to the minus root in (2.39c), (2.36d), and (2.41), is such that $s_g > 1$. Therefore, on this branch the GS model is spectrally equivalent to the GM model with an exponent set $(2,s_g,2,s_g)$ that satisfies (1.5). Since $0 < s_g < 1$ hold on the lower branch, we must allow for $\zeta < 0$ in the GM model in our spectral equivalence principle.

3 Analysis of Nonlocal Eigenvalue Problem: Instabilities

We now analyze the nonlocal eigenvalue problems in Principal Results 2.1–2.4 to determine specific conditions for which an instability occurs on an $O(1)$ time-scale. With the equivalence principle of Principal Result 2.5, in the remainder of this paper we restrict the analysis to a comparison of the stability properties of quasi-equilibrium solutions for the GS model and the GM model for an exponent set where $(p,q,m,s) = (2,1,2,0)$. With this restriction, all of the nonlocal eigenvalue problems in Principal Results 2.1–2.4 can be written in terms of the multiplier χ by

$$L_0\Phi - \chi w^2 J = \lambda\Phi, \qquad J \equiv \frac{\int_{-\infty}^{\infty} w\Phi\,dy}{\int_{-\infty}^{\infty} w^2\,dy}. \tag{3.1}$$

Here the local operator L_0 is $L_0\Phi \equiv \Phi'' - \Phi + 2w\Phi$. We then let $\psi(y)$ be the solution to

$$L_0\psi \equiv \psi'' - \psi + 2w\psi = \lambda\psi + w^2\,, \qquad \psi \to 0 \quad \text{as} \quad |y| \to \infty\,, \tag{3.2}$$

so that $\Phi = \chi J\psi$. We substitute this formula for Φ into the definition of J and assume that $J \neq 0$, so that we exclude the odd eigenfunction of L_0 that corresponds to a zero eigenvalue. In this way, we obtain that the eigenvalues of (3.1) satisfy $g(\lambda) = 0$, where

$$g(\lambda) \equiv C(\lambda) - f(\lambda)\,, \qquad C(\lambda) \equiv 1/\chi, \qquad f(\lambda) \equiv \frac{\int_{-\infty}^{\infty} w\,(L_0 - \lambda)^{-1}\, w^2\, dy}{\int_{-\infty}^{\infty} w^2\, dy}\,. \tag{3.3}$$

In (3.3), the multiplier χ can take any one of the four expressions given in Principal Results 2.1–2.4. From Principal Results 2.1–2.4 there are four expressions for C, which we write here as

$$C_{gs}(\lambda) \equiv \frac{1}{2} + \frac{\sqrt{1+\tau\lambda}}{2s_g}\left(\frac{\beta(\theta_\lambda;x_0)}{\beta(\theta_0;x_0)}\right)\,, \qquad C_{gm}(\lambda) \equiv \frac{\sqrt{1+\tau\lambda}}{2}\left(\frac{\beta(\theta_\lambda;x_0)}{\beta(\theta_0;x_0)}\right)\,, \tag{3.4a}$$

$$C_{gs\pm} \equiv \frac{1}{2} + \frac{\sqrt{1+\tau\lambda}}{2s_g}\left(\frac{\kappa_\pm(\tau\lambda)}{\kappa_+(0)}\right)\,, \qquad C_{gm\pm} \equiv \frac{\sqrt{1+\tau\lambda}}{2}\left(\frac{\kappa_\pm(\tau\lambda)}{\kappa_+(0)}\right)\,. \tag{3.4b}$$

Here $\beta(\xi;\theta_0)$ and $\kappa_\pm(\tau\lambda)/\kappa_+(0)$ were defined in (2.45) and (2.34). The first and second rows in (3.4) above correspond to one-spike and two-spike quasi-equilibria for the GS and GM models, respectively. Notice that for two-spike quasi-equilibria the GS and GM models each have two multipliers.

3.1 Some General Spectral Properties

To determine the zeroes of $g(\lambda)$ in the unstable right half-plane $\mathrm{Re}(\lambda) > 0$ we must first characterize the spectrum of L_0. The following result of [24] and [6] shows that $g(\lambda)$ has a simple pole in $\mathrm{Re}(\lambda) > 0$:

Proposition 3.1: (From [24] and [6]): *Consider the local eigenvalue problem $L_0\phi_l = \mu\phi_l$ for $\phi_l(y) \in \mathcal{H}^1$ on $-\infty < y < \infty$. This problem admits three discrete eigenvalues $\mu_0 = 5/4$, $\mu_1 = 0$, and $\mu_2 = -3/4$. The corresponding principal eigenfunction ϕ_{l0} has one sign.*

To determine a bound on the number of roots of (3.3) in $\mathrm{Re}(\lambda) > 0$ we calculate the winding number of $g(\lambda) = C(\lambda) - f(\lambda)$ with $\lambda = \lambda_R + i\lambda_I$ over the counterclockwise contour composed of the imaginary axis $-iR \le \mathrm{Im}\lambda \le iR$ and the semi-circle Γ_R, given by $|\lambda| = R > 0$, for $-\pi/2 \le \arg\lambda \le \pi/2$. Here $C(\lambda)$ is any one of the four expressions in (3.4). Assuming that there are no zeros of $g(\lambda)$ on the imaginary axis, we let $R \to \infty$ and use the argument principle to determine the number of zeros of $g(\lambda)$ in the right half-plane. From Proposition 3.1, $g(\lambda)$ is analytic in the right half-plane except at the simple pole $\lambda = \mu_0 = 5/4 > 0$. In addition, for any $\tau > 0$, we have from (3.4) that $C(\lambda) \sim O(\sqrt{\lambda})$ as $|\lambda| \to \infty$ in the right half-plane for any one of the four expressions for C. Since, in addition, $f(\lambda) \to 0$ as $|\lambda| \to \infty$, we obtain that the change in the argument of $g(\lambda)$ over Γ_R as $R \to \infty$ is $\pi/2$ for any $\tau > 0$. This leads to the following winding number criterion for the number M of unstable eigenvalues:

Proposition 3.2: *Let $\tau > 0$ and assume that there are no zeros of $g(\lambda)$ on the imaginary axis. Then, the total number of roots of (3.3) in the unstable right half-plane $Re(\lambda) > 0$ satisfies*

$$M = \frac{5}{4} + \frac{1}{\pi}\left[\arg g\right]_{\Gamma_I}\,, \quad \text{for} \quad k = 1\,; \qquad M = \frac{5}{2} + \frac{1}{\pi}\left(\left[\arg g_+\right]_{\Gamma_I} + \left[\arg g_-\right]_{\Gamma_I}\right)\,, \quad \text{for} \quad k = 2\,. \tag{3.5}$$

Here g is either g_{gs} or g_{gm}, $g_\pm$ is either $g_{gs\pm}$ or $g_{gm\pm}$, and $[arg\, g]_{\Gamma_I}$ is the change in the argument of $g(\lambda)$ along the semi-infinite imaginary axis $\Gamma_I \equiv i\lambda_I$, $\lambda_I \geq 0$, traversed in the downwards direction.

To evaluate M from (3.5) we need some properties of $g(\lambda)$ on $\lambda = i\lambda_I$, where $\lambda_I \geq 0$. Substituting $\lambda = i\lambda_I$ into (3.3) and (3.4), and extracting real and imaginary parts, we obtain that the roots of $g = 0$ on the imaginary axis are the roots of the coupled system $g_R = g_I = 0$, where

$$g_R(\lambda_I) \equiv C_R(\lambda_I) - f_R(\lambda_I)\,, \qquad g_I(\lambda_I) \equiv C_I(\lambda_I) - f_I(\lambda_I)\,, \tag{3.6a}$$

$$f_R(\lambda_I) \equiv \frac{\int_{-\infty}^{\infty} wL_0\left[L_0^2 + \lambda_I^2\right]^{-1} w^2\, dy}{\int_{-\infty}^{\infty} w^2\, dy}\,, \qquad f_I(\lambda_I) \equiv \frac{\lambda_I \int_{-\infty}^{\infty} w\left[L_0^2 + \lambda_I^2\right]^{-1} w^2\, dy}{\int_{-\infty}^{\infty} w^2\, dy}\,. \tag{3.6b}$$

Here $g_R(\lambda_I) \equiv \mathrm{Re}\left[g\left(i\lambda_I\right)\right]$, $g_I(\lambda_I) \equiv \mathrm{Im}\left[g\left(i\lambda_I\right)\right]$, $C_R(\lambda_I) \equiv \mathrm{Re}\left[C\left(i\lambda_I\right)\right]$, and $C_I(\lambda_I) \equiv \mathrm{Im}\left[C\left(i\lambda_I\right)\right]$.

Next, we summarize some key properties of the functions f_R, f_I, C_R, and C_I.

Proposition 3.3: *The functions f_R and f_I in (3.6b) have the asymptotic behavior*

$$f_R(\lambda_I) \sim 1 - \kappa_c\lambda_I^2 + O(\lambda_I^4)\,, \quad \text{as} \quad \lambda_I \to 0\,; \qquad f_R(\lambda_I) = 0\left(\lambda_I^{-2}\right)\,, \quad \text{as} \quad \lambda_I \to \infty\,, \tag{3.7a}$$

$$f_I(\lambda_I) \sim \frac{3\lambda_I}{4} + O(\lambda_I^3)\,, \quad \text{as} \quad \lambda_I \to 0\,; \qquad f_I(\lambda_I) = 0\left(\lambda_I^{-1}\right)\,, \quad \text{as} \quad \lambda_I \to \infty\,. \tag{3.7b}$$

Here $\kappa_c \equiv \int_{-\infty}^{\infty}\left(L_0^{-1}w\right)^2\, dy / \int_{-\infty}^{\infty} w^2\, dy > 0$. Moreover, $f_R(\lambda_I)$ and $f_I(\lambda_I)$ have the global behavior

$$f_R'(\lambda_I) < 0\,, \quad f_I(\lambda_I) > 0\,, \quad \text{for} \quad \lambda_I > 0\,. \tag{3.7c}$$

For any of the four expressions for C from (3.4), we have that

$$C_I(0) = 0\,; \quad C_R'(\lambda_I) > 0\,, \quad C_I'(\lambda_I) > 0\,, \quad \text{for} \quad \lambda_I > 0\,, \tag{3.8a}$$

$$C_R'(\lambda_I) = O(\tau^{1/2})\,, \quad C_I'(\lambda_I) = O(\tau^{1/2})\,, \quad \text{as} \quad \tau \to \infty\,, \quad \text{for} \quad \lambda_I > 0\,. \tag{3.8b}$$

Proof: The proof of the results in (3.7) are a special case of Propositions 3.1 and 3.2 of [42] corresponding to setting $(p, q, m, s) = (2, 1, 2, 0)$ in the GM model (1.4). The proof of (3.8) follows from setting $\lambda = i\lambda_I$ in any of the four expressions for $C(\lambda)$ in (3.4). ■

Using the properties given in Propositions 3.3, there are only a few possible values for $[\arg g]_{\Gamma_I}$. This leads to a more specific winding number criterion.

Proposition 3.4: *Let $\tau > 0$. Then, there are three distinct possibilities for $[arg\, g]_{\Gamma_I}$:*

$$(1)\text{:} \quad \text{if} \quad g_I < 0 \quad \text{when} \quad g_R = 0\,, \qquad \text{then} \quad [\arg g]_{\Gamma_I} = -5\pi/4\,, \tag{3.9a}$$

$$(2)\text{:} \quad \text{if} \quad g_I > 0 \quad \text{when} \quad g_R = 0\,, \qquad \text{then} \quad [\arg g]_{\Gamma_I} = 3\pi/4\,, \tag{3.9b}$$

$$(3)\text{:} \quad \text{if} \quad g_R > 0 \quad \text{for all} \quad \lambda_I \geq 0\,, \qquad \text{then} \quad [\arg g]_{\Gamma_I} = -\pi/4\,. \tag{3.9c}$$

Proof: Let $\tau > 0$. The properties of f_R and C_R show that $g_R = 0$ has at most one root. In addition, $\arg g = \pi/4$ as $\lambda_I \to +\infty$. Suppose that $0 < C_R(0) < f_R(0) = 1$ so that $g_R < 0$ and $g_I = 0$ at $\lambda_I = 0$.

Then, $\arg g = -\pi$ at $\lambda_I = 0$. Since the root to $g_R = 0$ is unique, this shows that $[\arg g]_{\Gamma_I}$ is either $5\pi/4$ or $-3\pi/4$ depending on the sign of g_I at the unique root of $g_R = 0$. This proves (3.9a) and (3.9b). Next, suppose that $C_R(0) > f_R(0) = 1$. Then, since $g_R(0) > 0$ and $g_R'(\lambda_I) > 0$, we conclude that $g_R > 0$ for $\lambda_I \geq 0$. In this case, $\arg g = 0$ at $\lambda_I = 0$. Since $g_R > 0$ for all $\lambda_I > 0$, (3.9c) follows. ■

Note that criterion (1) of Proposition 3.4 holds when $0 < C_R(0) < 1$ and τ is sufficiently small. Alternatively, if $0 < C_R(0) < 1$ and τ is sufficiently large, then criterion (2) holds. Criterion (3) holds when $C_R(0) > 1$. For a two-spike solution these results are used below as follows: If $C_{gs\pm}(0) < 1$ or $C_{gm\pm}(0) < 1$, we have either $M = 0$, $M = 2$, or $M = 4$ from (3.5) of Proposition 3.2. Alternatively, if $C_{gs+}(0) < 1$ and $C_{gs-}(0) > 1$, we have either $M = 1$ or $M = 3$ from (3.5).

For a one-spike solution we have from (3.4a) that $C_{gm}(0) = 1/2$ and $C_{gs}(0) = (s_g + 1)/(2s_g)$. Notice that $C_{gs}(0) < 1$ for $s_g > 1$. Therefore, from Propositions 3.2–3.4 we have for the GM model, and for the GS model with $s_g > 1$, that either $M = 0$ or $M = 2$. In this case, we will show below in §3.3 that there is a Hopf bifurcation for some $\tau = \tau_H$, which depends on x_0 and on D. Next, consider a one-spike solution to the GS model on the lower branch of the $|\nu|_2$ versus $\mathcal{A}$ bifurcation diagram where $0 < s_g < 1$. In this case, $C_{gs}(0) > 1$, and so since condition (3.9c) of Proposition 3.4 holds, we get from Proposition 3.2 that $M = 1$. Hence, a one-spike solution for the GS model with $0 < s_g < 1$ is unstable.

Next, we analyze the zeroes of $g(\lambda) = 0$ on the real positive axis. The following result characterizes the behavior of $f(\lambda)$ and $C(\lambda)$ on the positive real axis.

Proposition 3.5: (From [42]): *For $\lambda = \lambda_R \geq 0$ and real, $f(\lambda_R)$ in (3.3) has the local behavior*

$$f(\lambda_R) \sim 1 + \frac{3\lambda_R}{4} + \kappa_c \lambda_R^2, \quad \text{as} \quad \lambda_R \to 0; \qquad \kappa_c \equiv \frac{\int_{-\infty}^{\infty} \left(L_0^{-1} w\right)^2 \, dy}{\int_{-\infty}^{\infty} w^2 \, dy}, \tag{3.10a}$$

and $f(\lambda_R) \to +\infty$ as $\lambda_R \to \mu_0^-$. In addition, we have the global behavior

$$f'(\lambda_R) > 0 \quad \text{and} \quad f''(\lambda_R) > 0, \quad \text{for} \quad 0 < \lambda_R < \mu_0. \tag{3.10b}$$

On the other side of the singularity we have $f(\lambda_R) < 0$ for $\lambda_R > \mu_0$. Moreover, for each of the four choices for C in (3.4), we have for $\lambda_R > 0$ that $C(\lambda_R)$ is a positive, increasing, and concave function

$$C'(\lambda_R) > 0, \qquad C''(\lambda_R) < 0, \qquad C'(\lambda_R) = O(\tau^{1/2}), \quad \text{as} \quad \tau \to +\infty. \tag{3.10c}$$

Proof: This result for $f(\lambda_R)$ is simply Proposition 3.5 of [42] for a GM model with exponents $(p, q, m, s) = (2, 1, 2, 0)$. The result (3.10c) follows from a simple exercise in calculus (see equations (3.38)–(3.41) of [42] where a similar calculation was done for equilibrium solutions to the GM model (1.4)). ■

These properties of $f(\lambda)$ and $C(\lambda)$ show that, for any $\tau > 0$, there is exactly one root to $g(\lambda) = 0$ on the positive real axis when $C(0) > 1$. By Propositions 3.2–3.4 this is the only root in $\mathrm{Re}(\lambda) > 0$. Alternatively, if $0 < C(0) < 1$, we conclude from Proposition 3.5 that there are exactly two such roots to $g(\lambda) = 0$ on the positive real axis for τ sufficiently large and no roots for τ sufficiently small.

3.2 Competition Instabilities

We now examine instabilities that occur as a result of a unique real positive eigenvalue. As discussed above, for a one-spike solution this instability is only possible for the GS model with $0 < s_g < 1$. However, for two-spike solutions, we now show that this instability can occur for both the GS and the GM models in certain parameter regimes. For a two-spike solution, we show that this instability can only arise from C_{gs-} and C_{gm-} in (3.4). Since, from (2.37c), the onset of this instability conserves the sum of the amplitudes of the spikes, we call it a *competition instability.*

We first analyze competition instabilities for a two-spike solution for the GM model (1.4). From (3.4) we calculate that $C_{gm+}(0) < 1$ for any $\alpha > 0$ and $D > 0$. Recall that 2α is the distance between the two spikes. From Propositions 3.2–3.5, we have for τ sufficiently small that there are no roots of $g_{gm+}(\lambda) = 0$ in $\mathrm{Re}(\lambda) > 0$ and two such roots when τ is sufficiently large. However, if $\kappa_-(0)/\kappa_+(0) > 2$, we have that $C_{gm-}(0) > 1$. In this case, we see from Proposition 3.5 that there is exactly one real positive root of $g_{gm-}(\lambda) = 0$ in the right half-plane for any $\tau > 0$. Hence, taking into account both signs of $g_{gm\pm}$, we have that $M = 1$ for τ sufficiently small and $M = 3$ for τ sufficiently large. By using (3.4) for $C_{gm-}(0)$ and (2.34) for $\kappa_-(0)/\kappa_+(0)$, a simple calculation shows that there is a competition instability for τ sufficiently small when

$$G(\alpha;\theta_0) > 2\,, \qquad G(\alpha;\theta_0) \equiv \coth(\theta_0)\coth(\theta_0\alpha)\,. \tag{3.11}$$

By differentiating G, we obtain that $G_\alpha < 0$ for $\alpha > 0$, and so G has its minimum on $0 < \alpha \le 1$ at $\alpha = 1$. Therefore, if $G(1;\theta_0) > 2$, we have a competition instability for any α in $0 < \alpha < 1$. Setting $G(1;\theta_0) = 2$, and solving for D, we obtain the following result:

Proposition 3.6: *Consider a two-spike quasi-equilibrium solution for the GM model (1.4) as given in Principal Result 2.3. Suppose that* $0 < D < D_* \equiv \left[\log(\sqrt{2}+1)\right]^{-2} \approx 1.287$ *and* $0 \le \tau < \tau_H$ *for some* $\tau_H > 0$. *Define* α_c *in* $0 < \alpha_c < 1$ *by*

$$\alpha_c \equiv \frac{1}{2\theta_0}\log\left[\frac{2+\coth\theta_0}{2-\coth\theta_0}\right]\,, \qquad \theta_0 = D^{-1/2}\,. \tag{3.12}$$

Then, for any α *with* $0 < \alpha < \alpha_c$, *the quasi-equilibrium solution is unstable as a result of a unique eigenvalue in* $Re(\lambda) > 0$ *located on the positive real axis. Alternatively, for* $\alpha_c < \alpha < 1$, *and for* $0 \le \tau < \tau_H$, *the two-spike solution is stable on an* $O(1)$ *time-scale. As* $D \to 0$, *but with* $D \gg O(\varepsilon^2)$, *we have* $\alpha_c \sim \frac{\sqrt{D}}{2}\log 3$ *so that the zone of stability* $O(\varepsilon) \ll O(\sqrt{D}) \ll \alpha < 1$ *almost covers the entire range* $0 < \alpha < 1$. *Finally, for* $D > D_* \approx 1.287$, *the two-spike quasi-equilibrium solution is unstable for any* α *with* $0 < \alpha < 1$, *and for any* $\tau > 0$.

In Fig. 3(a) we plot $G(\alpha;\theta_0)$ versus α for several values of D. In Fig. 3(b) we plot D versus α_c. An interesting dynamical behavior occurs when $\alpha_c > 1/2$. Setting $\alpha_c = 1/2$ in (3.12), and solving for $D = D_2$, we calculate that

$$D_2 = \left[\log(2+\sqrt{3})\right]^{-2} \approx 0.5765\,. \tag{3.13}$$

Therefore, for D satisfying $D_2 < D < D_*$, a competition instability will occur for any α with $0 < \alpha < \alpha_c$, where $\alpha_c > 1/2$. As seen from (2.42d) of Principal Result 2.3, the dynamics of a two-spike solution

is such that $\alpha(t) \to 1/2$ as $t \to \infty$ on the long time-scale $t = O(\varepsilon^{-2})$ for any initial condition $\alpha(0)$. However, when the initial spike location $\alpha(0)$ satisfies $\alpha_c < \alpha(0) < 1$, with $\alpha_c > 1/2$, we have that $\alpha(t)$ slowly decreases as t increases, with speed $O(\varepsilon^2)$, and will eventually cross below the stability threshold α_c before it reaches a neighborhood of the equilibrium point $\alpha = 1/2$. Once α decreases below α_c, the two-spike quasi-equilibrium solution is subject to a competition instability that occurs on an $O(1)$ time-scale. This time-scale is fast compared to the time-scale of the spike motion. Since this instability is associated with the dynamics of slowly moving spikes, and is triggered at later times, it is referred to here as a *dynamic competition instability*. This instability is illustrated numerically in §4.

Qualitatively, a dynamic competition instability occurs when a slowly moving spike that is initially stable at $t = 0$ enters into an unstable zone at some later time $t = O(\varepsilon^{-2})$ before it reaches a neighborhood of its equilibrium value at $\alpha = 1/2$. This dynamic phenomenon is distinct from a static competition instability that occurs immediately at $t = 0$ when the spike location is initially in the unstable zone. Therefore, this shows that spikes that are initially stable can be destabilized at later times as a result of their mutual interaction or their interaction with the boundary.

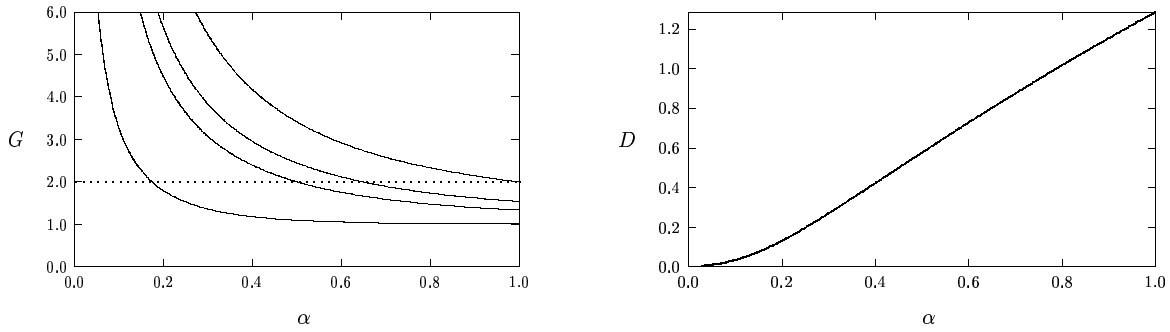

(a) $G(\alpha;\theta_0)$ versus α (b) D versus α_c

Figure 3: Left figure: $G(\alpha;\theta_0)$ versus α, given in (3.11), for $D = 0.1$ (bottom curve), $D = 0.5765$, $D = 0.8$, and $D = 1.287$ (top curve). Note that G is an increasing function of D, and when G is above the dotted curve we have instability. Right figure: D versus α_c, defined in (3.12). For $0 < D < D_* = 1.287$, we have $0 < \alpha_c < 1$. Above this curve we have a competition instability.

A similar analysis can be done for the GS model. We first note that $C_{gs\pm}(0) > 1$ when $0 < s_g < 1$. In this case, Propositions 4.2–4.5 show that there are exactly two unstable, and real, eigenvalues in the right half-plane for any $\tau > 0$. Hence, the lower branch of the bifurcation diagram of $|\nu_2|$ versus $\mathcal{A}$, corresponding to the positive root in (2.41), is always unstable.

For $s_g > 1$, we get $C_{gs+}(0) < 1$. Hence, from Propositions 3.2–3.5, there are no roots of $g_{gs+}(\lambda) = 0$ in $\mathrm{Re}(\lambda) > 0$ when τ is sufficiently small and two such roots when τ is sufficiently large. However, $C_{gs-}(0) > 1$ when $\kappa_-(0)/\kappa_+(0) \equiv \coth\theta_0 \coth(\theta_0\alpha) > s_g$. In this case, Proposition 3.5 shows that there

is a unique real positive root of $g_{gs-}(\lambda) = 0$ for any $\tau > 0$. Since criterion (3) of Proposition 3.4 holds, we get from (3.5) that this is the only root of $g_{gs-} = 0$ in $\mathrm{Re}(\lambda) > 0$. Therefore, including both signs $g_{gs\pm}$, we conclude that $M = 1$ for τ sufficiently small and $M = 3$ for τ sufficiently large. To express this stability result in terms of $\mathcal{A}$, we use (2.36d) to obtain

$$\mathcal{A} = \mathcal{A}_{2e}\frac{(1+s_g)}{2\sqrt{s_g}}. \tag{3.14}$$

Substituting the stability threshold $\coth\theta_0 \coth(\theta_0\alpha) = s_g$ into (3.14), and noting that $(1+s_g)/\sqrt{s_g}$ is an increasing function of s_g for $s_g > 1$, we obtain the following result:

Proposition 3.7: *Consider a two-spike quasi-equilibrium solution for the GS model (1.3) as given in Principal Result 2.1. This solution is unstable on the lower branch of the $|\nu|_2$ versus $\mathcal{A}$ bifurcation diagram, where $0 < s_g < 1$. Now consider the upper branch of this diagram where $s_g > 1$. Then, for $0 \le \tau < \tau_H$ for some $\tau_H > 0$, and for $\mathcal{A}_{2e} < \mathcal{A} < \mathcal{A}_{2L}$, where $\mathcal{A}_{2e}$ is the existence threshold of (2.35), the quasi-equilibrium solution is unstable as a result of a unique eigenvalue in $Re(\lambda) > 0$ located on the positive real axis. The threshold $\mathcal{A}_{2L}$ is given by*

$$\mathcal{A}_{2L} \equiv \mathcal{A}_{2e}\frac{[1+\coth(\theta_0)\coth(\theta_0\alpha)]}{2\sqrt{\coth(\theta_0)\coth(\theta_0\alpha)}}. \tag{3.15}$$

Alternatively, for $0 < \tau < \tau_H$, the solution is stable on an $O(1)$ time-scale when $\mathcal{A} > \mathcal{A}_{2L}$.

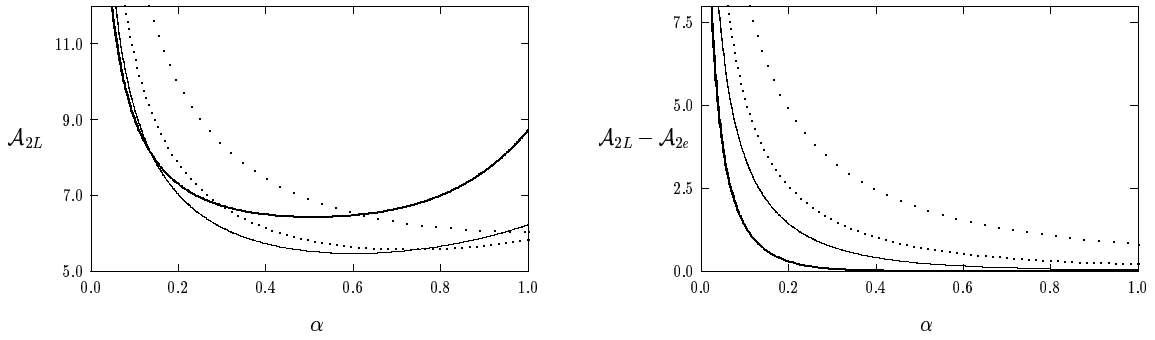

(a) $\mathcal{A}_{2L}$ versus α (b) $\mathcal{A}_{2L} - \mathcal{A}_{2e}$ versus α

Figure 4: Left figure: the stability threshold $\mathcal{A}_{2L}$ versus α for four values of D. Right figure: the difference $\mathcal{A}_{2L} - \mathcal{A}_{2e}$ versus α for the same four values of D. Here $D = 0.1$ (heavy solid curve), $D = 0.5$ (solid curve), $D = 1.0$ (dotted curve), and $D = 2.306$ (widely spaced dots).

In Fig. 4(a) and Fig. 4(b) we plot $\mathcal{A}_{2L}$ and the difference $\mathcal{A}_{2L} - \mathcal{A}_{2e}$ versus α, respectively, for four values of D. A competition instability occurs at time $t = 0$ when $\mathcal{A}$ satisfies $\mathcal{A}_{2e} < \mathcal{A} < \mathcal{A}_{2L}$ for the initial value $\alpha = \alpha(0)$. These plots show that for D small, the stability and existence thresholds are

close in value except when the two spikes are close together. Therefore, when $D \ll 1$, and when the two spikes are not too close at $t = 0$, the interval in $\mathcal{A}$ where competition instabilities exist at time $t = 0$ is quite narrow. Alternatively, for $D \gg 1$, then for each initial location $\alpha(0)$ there is a much wider interval in $\mathcal{A}$ where this instability occurs at $t = 0$. For three values of α, in Fig. 5(a) we plot the bifurcation diagram $|\nu|_2$, defined in (2.41), versus $\mathcal{A}$ for $D = 0.1$. A similar plot is shown in Fig. 5(b) for $D = 1.0$. In these figures, the dotted lines indicate the portions of the branches that are unstable when $\tau = 0$.

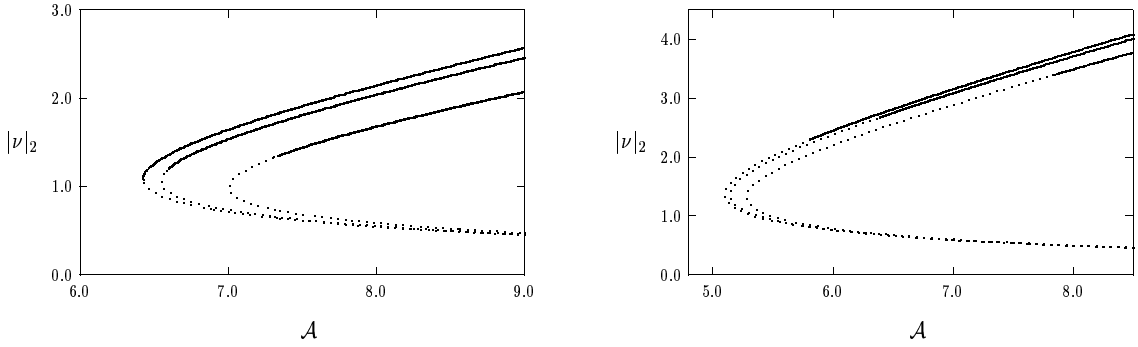

(a) $D = 0.1$ (b) $D = 1.0$

Figure 5: The bifurcation diagram $|\nu|_2$, defined in (2.41), versus $\mathcal{A}$ for $\alpha = 0.2$ (rightmost curve), $\alpha = 0.35$ (middle curve), and $\alpha = 0.5$ (leftmost curve). Those portions that are unstable due to a competition instability correspond to the dotted lines. Left figure: $D = 0.1$. Right figure: $D = 1.0$.

Next, we determine the range of parameters where dynamic competition instabilities can occur for a slowly drifting two-spike pattern. We assume that there is no competition instability at $t = 0$. To determine where a dynamic instability occurs we must first study the monotonicity property of $\mathcal{A}_{2L}$ as a function of α. Upon differentiating (3.15) with respect to α, and using (2.35) for $\mathcal{A}_{2e}$ as a function of α, we obtain after a lengthy but straightforward calculation that

$$\frac{d\mathcal{A}_{2L}}{d\alpha} = E(\alpha)H(2\theta_0\alpha)\,, \quad E(\alpha) \equiv \sqrt{\frac{12\theta_0^3}{\sinh\theta_0}}\frac{\cosh\left[\frac{1}{2}\log\left(\coth\theta_0\coth(\theta_0\alpha)\right)\right]}{\left(\cosh\theta_0+\cosh\left[2\theta_0\left(\alpha-1/2\right)\right]\right)^{1/2}}\,, \tag{3.16a}$$

where $H(y)$, with $y = 2\theta_0\alpha$, is defined by

$$H(y) \equiv \sinh(y-\theta_0) - \frac{\left(\cosh\theta_0+\cosh(y-\theta_0)\right)^2}{\sinh(y)\left(\cosh\theta_0+\cosh(y+\theta_0)\right)}\,. \tag{3.16b}$$

Since $E > 0$ for $\alpha > 0$ and $H(y) < 0$ for $0 < y < \theta_0$, (3.16) shows that $d\mathcal{A}_{2L}/d\alpha < 0$ for $0 < \alpha < 1/2$. Therefore, $\mathcal{A}_{2L}$ is always decreasing on $0 < \alpha < 1/2$ for any $D > 0$ (see Fig. 4(a)). In addition, since $H(\theta_0) < 0$, $\mathcal{A}_{2L}$ is also decreasing on some interval to the right of $\alpha = 1/2$ for any $D > 0$. We now determine a critical value of D, labeled by D_{2gs}, for which $d\mathcal{A}_{2L}/d\alpha < 0$ on $0 < \alpha < 1$ whenever

$D > D_{2gs}$. To determine this value we first note that $H(y)$ is an increasing function of y in $\theta_0 < y < 2\theta_0$. Therefore, the critical value D_{2gs} is obtained by setting $H(2\theta_0) = 0$, which enforces $d\mathcal{A}_{2L}/d\alpha = 0$ at $\alpha = 1$. Setting $H(2\theta_0) = 0$, we get

$$\sinh\theta_0 = \frac{4\cosh^2(\theta_0)}{\sinh(2\theta_0)\left(\cosh\theta_0 + \cosh(3\theta_0)\right)}\,. \tag{3.17}$$

This equation can be rewritten as $\sinh^2\theta_0 = \left(2\sinh^2\theta_0 + 1\right)^{-1}$. Solving this quadratic equation, and setting $D = \theta_0^{-2}$, we get the critical value

$$D_{2gs} \equiv \left[\log\left(\frac{1}{\sqrt{2}} + \sqrt{\frac{3}{2}}\right)\right]^{-2} \approx 2.3063\,. \tag{3.18}$$

Therefore, when $D > D_{2gs}$, $\mathcal{A}_{2L}$ is monotone decreasing on $0 < \alpha < 1$. The widely spaced dotted curve in Fig. 4(a) is shown at this value $D = D_{2gs} \approx 2.3063$. Next, we show that this monotonicity result for $\mathcal{A}_{2L}$ leads to dynamic competition instabilities whenever $1/2 < \alpha(0) < 1$.

Proposition 3.8: *Consider a two-spike quasi-equilibrium solution for the GS model (1.3) as given in Principal Result 2.1. Suppose that the initial spike location $\alpha(0)$ satisfies $1/2 < \alpha(0) < 1$, and that $D > D_{2gs} \approx 2.3063$. Let $\mathcal{A}_{2L}(1/2)$ and $\mathcal{A}_{2L}(\alpha(0))$ denote the stability thresholds for the equilibrium spike location $\alpha = 1/2$ and for the initial location $\alpha(0)$. Next, suppose that $\mathcal{A}$ satisfies $\mathcal{A}_{2L}(\alpha(0)) < \mathcal{A} < \mathcal{A}_{2L}(1/2)$. Then, the slowly modulated two-spike solution will experience a dynamic competition instability at a later time before reaching the vicinity of the equilibrium location $\alpha = 1/2$.*

Notice that for any $0 < D < D_{2gs}$ we can still have dynamic competition instabilities for a certain range of initial spike locations $\alpha(0)$ with $\alpha(0) > 1/2$. This follows since $d\mathcal{A}_{2L}/d\alpha < 0$ at $\alpha = 1/2$ for any $D > 0$. All that is required for this instability is that $d\mathcal{A}_{2L}/d\alpha < 0$ on $1/2 < \alpha < \alpha(0)$ and that $\mathcal{A}$ is chosen in the range $\mathcal{A}_{2L}(\alpha(0)) < \mathcal{A} < \mathcal{A}_{2L}(1/2)$. Notice also that since $d\mathcal{A}_{2L}/d\alpha < 0$ on $0 < \alpha < 1/2$, a dynamic competition instability is not possible for any initial spike location with $0 < \alpha(0) < 1/2$.

3.3 Oscillatory Instabilities

For each of the nonlocal eigenvalue problems in Principal Results 2.1–2.4, we now compute the minimum value of τ, labeled by τ_H, where there is a complex conjugate pair of eigenvalues on the imaginary axis. To determine τ_H, we compute the solution ψ to (3.2) using a boundary-value solver, and then use Newton's method to look for roots of (3.6). A similar method was used in [42] to determine stability thresholds for k-spike equilibria of the GM model (1.4).

We begin by considering a one-spike solution to the GM model. Let M denote the number of unstable eigenvalues. Since $C_{gm}(0) < 1$, we conclude from Propositions 3.2–3.5 that $M = 0$ when $0 < \tau < \tau_H$, and $M = 2$ when $\tau \gg 1$. In Fig. 6(a), we plot the numerically computed τ_H versus α for different values of D. Although, we are not able to prove that τ_H is unique, numerically we find that there are exactly two eigenvalues in $\mathrm{Re}(\lambda) > 0$ for any $\tau > \tau_H$. Since, under (2.44b), the spike tends to the origin over a time-scale $t = O(\varepsilon^{-2})$, the monotone increasing behavior of τ_H for the larger values of

D in Fig. 6(a) show that a *dynamic oscillatory instability* can occur. Such an instability occurs when a spike, initially located at $\alpha(0)$ at $t = 0$ where $\tau < \tau_H$, eventually enters into a region where $\tau > \tau_H$ as it slowly drifts towards the origin. An example of this instability is shown below in §4.

Next, consider a two-spike solution to the GM model. Suppose that $\alpha_c < \alpha < 1$, where α_c is competition instability threshold of (3.12). Since $C_{gm\pm}(0) < 1$, we have stability for $0 < \tau < \tau_H$, where

$$\tau_H = \min(\tau_{H-}, \tau_{H+}) \,. \tag{3.19}$$

Here $\tau_{H\pm}$ are the minimum values of τ where $g_{gm\pm}(\lambda) = 0$ has roots on the imaginary axis at $\lambda = i\lambda_{I\pm}$ with $\lambda_{I\pm} > 0$. By determining these roots numerically we find that the minimum in (3.19) occurs for C_{gm+}, so that $\tau_H = \tau_{H+}$. From (2.37c) it follows that this oscillatory instability synchronizes the amplitudes of the spikes at the onset of the instability. In Fig. 6(b) we plot τ_H versus α for various values of D. In this figure, the dotted portions of the curves are where $0 < \alpha < \alpha_c$, which correspond to regions where there is a competition instability for any $\tau > 0$. Since $\alpha \to 1/2$ as $t \to \infty$ under (2.42d), we again conclude from this figure that there can be a dynamic oscillatory instability when D is large enough. A numerical experiment to illustrate this instability is given in §4.

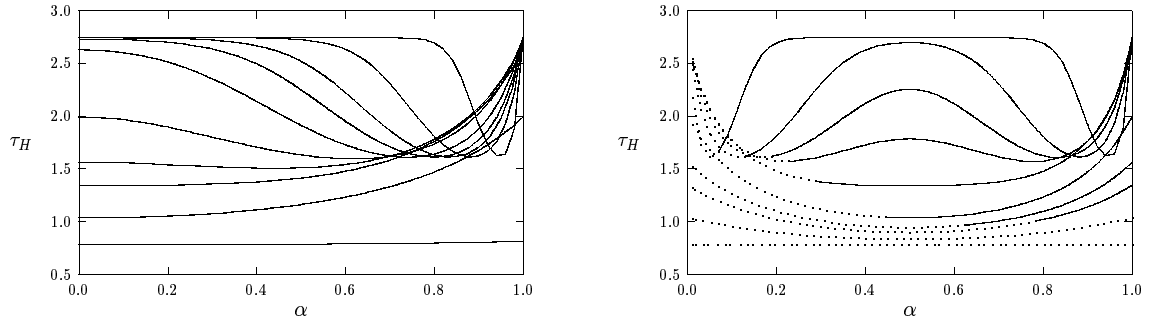

(a) one spike

(b) two spikes

Figure 6: Hopf bifurcation values τ_H versus α for various D for one-spike (left figure) and two-spikes (right figure). The values are $D = 50$, $D = 2$, $D = 1$, $D = 0.75$, $D = 0.5$, $D = 0.25$, $D = 0.15$, $D = 0.10$, $D = 0.05$, and $D = 0.01$. In the left figure, higher values of D correspond to lower y-intercepts. In the right figure, lower values of D correspond to higher values of τ_H at $\alpha = 1/2$. The dotted lines correspond to the segments $\alpha < \alpha_c$, where α_c is the competition instability threshold of (3.12).

For both one and two spike solutions, Fig. 6 suggests that τ_H lies between its limiting values for $D \ll 1$ and for $D \gg 1$. For $D \ll 1$, (3.4) yields that $C_{gm} \sim C_{gm+} \sim \frac{1}{2}\sqrt{1+\tau\lambda}$. The corresponding NLEP has a Hopf bifurcation at $\tau_H = 2.75$, which corresponds to a one-spike solution for the infinite-line problem (see Remark 3.10 of [42]). Alternatively, for $D \gg 1$, we get that $C_{gm} \sim C_{gm+} \sim \frac{1}{2}(1+\tau\lambda)$, which corresponds to the shadow GM model with exponent set $(p, q, m, s) = (2, 1, 2, 0)$. For this problem a Hopf bifurcation occurs when $\tau_H = 0.771$ (see Table 1 of [43]). This leads to a conjecture.

Conjecture 3.9: *Consider a one or two-spike quasi-equilibrium solution for the GM model, and let* $D > 0$. *Then, the value* τ_H *where complex conjugate eigenvalues are located on the imaginary axis satisfies* $0.771 < \tau_H < 2.75$. *The lower bound corresponds to the shadow limit* $D = \infty$, *while the upper bound corresponds to the infinite-line problem obtained by taking the limit* $D \to 0$ *(with* $D \gg O(\varepsilon^2)$*).*

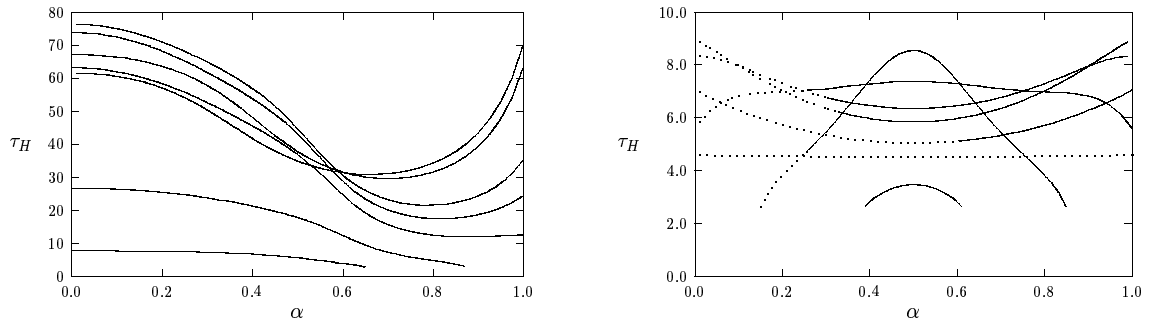

(a) one spike

(b) two spikes

Figure 7: Left figure: $\tau_H(\alpha)$ when $\mathcal{A} = 6.5$ for one spike and for different values of D. The curves, labeled by $(\tau_H(0), D)$, are: $(7.7, 0.1)$, $(26.7, 0.2)$, $(63.2, 0.5)$, $(73.9, 0.75)$, $(76.4, 1.0)$, $(67.3, 2.0)$, and $(61.6, 2.5)$. Right figure: $\tau_H(\alpha)$ when $\mathcal{A} = 6.5$ for two spikes and different values of D. The curves, labeled by $(\tau_H(1/2), D)$ are: $(3.47, 0.1)$, $(8.56, 0.2)$, $(7.39, 0.5)$, $(6.36, 0.75)$, $(5.84, 1.0)$, $(5.04, 2.25)$, and $(4.5, 50)$.

Next, we consider a one-spike solution to the GS model. In Fig. 7(a) we plot the numerically computed τ_H versus α for different values of D when $\mathcal{A} = 6.5$. In this figure, the curves for $D = 0.1$ and $D = 0.2$ terminate at some $\alpha < 1$ where $\mathcal{A} = \mathcal{A}_{1e}$. Recall from Fig. 1(a) that the existence threshold $\mathcal{A}_{1e}$ is monotonically increasing in α. In the regions where τ_H is an increasing function of α, we see from Fig. 7(a) the possibility of dynamic oscillatory instabilities for a one-spike solution that slowly drifts towards the origin under (2.39b).

Finally, we determine τ_H for a two-spike solution of the GS model. Suppose that $\mathcal{A} > \mathcal{A}_{2L}$, so that a two-spike solution is stable for $0 < \tau < \tau_H$, where τ_H is defined in (3.19). In (3.19), $\tau_{H\pm}$ now denotes the minimum values of τ where $g_{gs\pm}(\lambda) = 0$ has roots on the imaginary axis at $\lambda = i\lambda_{I\pm}$ with $\lambda_{I\pm} > 0$. As for the GM model, we again find that the minimum in (3.19) occurs for C_{gs+}, so that $\tau_H = \tau_{H+}$. This leads to the onset of a synchronous oscillatory instability in the spike amplitudes. In Fig. 7(b) we plot τ_H versus α for various values of D when $\mathcal{A} = 6.5$. The endpoints of the curves in this figure correspond to where $\mathcal{A} = \mathcal{A}_{2e}$. The dashed portions of the curves in Fig. 7(b) correspond to regions where $\mathcal{A}_{2e} < \mathcal{A} < \mathcal{A}_{2L}$, that lead to a competition instability for any $\tau > 0$. From this figure, we again see the possibility of dynamic oscillatory instabilities for a slowly drifting two-spike solution that satisfies $\alpha \to 1/2$ at $t \to \infty$ from (2.36c). These instabilities are illustrated in §4. In general, τ_H depends on $\mathcal{A}$, α, and D. Although, it can be readily computed for parameter values other than those

shown in the figures above, it is difficult to predict the qualitative behavior of τ_H with respect to these parameters. However, for $\mathcal{A} \gg 1$, we now show that τ_H has a simple scaling law behavior.

3.4 The Intermediate Regime of the Gray-Scott Model

In this section we consider the *intermediate* parameter regime for the GS model (1.1). Recalling that $A \equiv \varepsilon^{1/2}\mathcal{A}$ from (1.2), we define this regime for $D \ll O(1)$ by

$$O\left(\varepsilon^{1/2}D^{-1/4}\right) \ll A \ll O(1)\,, \qquad \to \qquad O\left(D^{-1/4}\right) \ll \mathcal{A} \ll O(\varepsilon^{-1/2})\,. \tag{3.20}$$

Alternatively, for $D = O(1)$, it is defined by $O(\varepsilon^{1/2}) \ll A \ll O(1)$, or equivalently by $O(1) \ll \mathcal{A} \ll O(\varepsilon^{-1/2})$. Since, from (2.38) and (2.35), we have $\mathcal{A}_{1e} = \mathcal{A}_{2e} = O(D^{-1/4})$ for $D \ll O(1)$, and $\mathcal{A}_{1e} = \mathcal{A}_{2e} = O(1)$ for $D = O(1)$ and $D \gg O(1)$, the intermediate regime provides the transition between the saddle-node bifurcation region, where $\mathcal{A} = O(\mathcal{A}_{ke})$, and the pulse-splitting region where $A = O(1)$ (cf. [18]). Notice also from (3.20) that as D decreases towards $D = O(\varepsilon^2)$, corresponding to the weak spike interaction regime of [31], [32], and [41], the intermediate regime disappears.

Letting $\mathcal{A}/\mathcal{A}_{ke} \gg 1$, and taking the minus root in (2.39c) and (2.36d), we obtain for $k = 1, 2$ that

$$s_g \sim \frac{4\mathcal{A}^2}{\mathcal{A}_{ke}^2} - 2 + o(1)\,, \qquad \text{for} \quad \mathcal{A}/\mathcal{A}_{ke} \gg 1\,. \tag{3.21}$$

Now for $s_g \gg 1$, we calculate from (3.4) that $C_{gs}(0) \sim C_{gs\pm}(0) \sim 1/2 < 1$. Therefore, there are no competition instabilities in the intermediate parameter regime. However, there can be a Hopf bifurcation when $\tau = O(s_g^2) \gg 1$. Letting $\tau \gg O(1)$ in (3.4), we calculate that

$$C_{gs} \sim \frac{1}{2}\left(1 + \sqrt{\tau\lambda}\frac{\omega_1}{s_g}\right)\,, \qquad C_{gs\pm} \sim \frac{1}{2}\left(1 + \sqrt{\tau\lambda}\frac{\omega_2}{s_g}\right)\,. \tag{3.22a}$$

Here, for one and two spikes, we have defined

$$\omega_1 = 2\left[\tanh(\theta_0(1+x_0)) + \tanh(\theta_0(1-x_0))\right]^{-1}\,, \quad \omega_2 = 2\left[\tanh(\theta_0\alpha) + \tanh(\theta_0(1-\alpha))\right]^{-1}\,. \tag{3.22b}$$

We then rescale τ by

$$\tau = \tau_0 s_g^2/\omega_k^2\,, \quad k = 1, 2\,. \tag{3.23}$$

Substituting (3.23) into (3.22a), we obtain $C_{gs} = C_{gs\pm} \sim \frac{1}{2}\left[1 + \sqrt{\tau_0\lambda}\right]$. Therefore, in the intermediate regime, we must study the following nonlocal eigenvalue problem:

$$L_0\Phi - \frac{2w^2}{1+\sqrt{\tau_0\lambda}}\left(\frac{\int_{-\infty}^{\infty} w\Phi\, dy}{\int_{-\infty}^{\infty} w^2\, dy}\right) = \lambda\Phi\,, \qquad -\infty < y < \infty\,, \qquad \Phi \to 0 \quad |y| \to \infty\,. \tag{3.24}$$

This NLEP has a much simpler form than the corresponding NLEP (2.37) of the low feed-rate regime.

The NLEP (3.24) was studied first in [4], [5], [27], and later in §4 of [17]. Numerical evidence shows that for any $\tau_0 > \tau_{0H}$, there are exactly two eigenvalues in the unstable right half-plane and that these eigenvalues merge onto the positive real axis at $\tau_0 = \tau_{0M} > \tau_{0H}$. They remain on the positive real axis

for $\tau_0 > \tau_{0M}$. For $\tau \to \infty$, one eigenvalue tends to the eigenvalue $\mu_0 = 5/4$ of the local operator L_0, while the other eigenvalue tends to zero. The existence of τ_{0H} and τ_{0M}, and the uniqueness of τ_{0M}, follows from using Propositions 3.2–3.5 (see also [17]). However, a rigorous proof of the uniqueness of τ_{0H} is an open problem. Numerical computations (see [4], [5], [17], [27]), yield the critical values

$$\tau_{0H} = 1.748\,, \qquad \tau_{0M} = 8.567\,. \tag{3.25}$$

Substituting (3.25) into (3.23), and using (3.21) together with (2.38) and (2.35) for $\mathcal{A}_{1e}$ and $\mathcal{A}_{2e}$, respectively, we obtain scaling laws for the Hopf bifurcation for a k-spike quasi-equilibrium solution

$$\tau_H = \frac{\tau_{0H}\mathcal{A}^4 D}{9\omega_k^4}\left(1 - \frac{6\omega_k}{\mathcal{A}^2\sqrt{D}}\right)^2 + o(1)\,, \qquad \to \qquad \tau_H = \frac{\tau_{0H}\varepsilon^{-2}A^4 D}{9\omega_k^4}\left(1 - \frac{6\varepsilon\omega_k}{A^2\sqrt{D}}\right)^2 + o(1)\,. \tag{3.26}$$

Here $A = \varepsilon^{1/2}\mathcal{A}$, and ω_k, for $k = 1, 2$, is defined in (3.22b) in terms of the spike locations.

A simple calculation using the leading-order term in (3.26) shows that τ_{0H} has its maximum value at the equilibrium locations $x_0 = 0$ and $\alpha = 1/2$ for a one-spike and a two-spike quasi-equilibrium solution, respectively. In addition, for $\mathcal{A} \gg O(1)$, τ_{0H} is convex, in x_0 and α. Therefore, there can be no dynamic oscillatory instabilities in the intermediate regime. In other words, if a one-spike or two-spike quasi-equilibrium is stable at $t = 0$ it will be stable on an $O(1)$ time-scale for all $t > 0$ under the flow (2.39b) and (2.36c), which ultimately drives the spikes to their equilibrium positions.

In the derivation of the ODE's (2.39b) and (2.36c) it was assumed that $\tau = O(1)$. Under this condition, the u_t term in (1.3b) is a higher-order correction term in both the inner region, representing the core of the spike, and in the outer region away from this core. However, in the intermediate regime we have from (3.26) that $\tau_H \gg 1$. Therefore, we must re-examine the analysis of §2 for asymptotically larger τ and determine a consistency condition for the validity of (2.39b) and (2.36c).

Consider a two-spike solution in the intermediate regime. Then, by letting $\mathcal{A} \gg 1$ in (2.36a) and (2.10), we have that $\nu = O\left(\mathcal{A}/{\mathcal{A}_{2e}}^2\right) \gg 1$ and $u = O\left(\mathcal{A}_{2e}^2/\mathcal{A}^2\right) \ll 1$ in the core of the spike. Upon using (3.21), the time-scale $\varepsilon^2 s_g\theta_0$ for the slow spike motion in (2.36c) becomes $O(\varepsilon^2\mathcal{A}^2)$. This suggests that in the intermediate regime, and in the core of the i^{th} spike, we look for a solution to (1.3) as

$$\nu_i(y,\sigma) = \mathcal{A}\nu_{i0} + \varepsilon\mathcal{A}^3\nu_{i1} + \cdots\,, \quad u_i(y,\sigma) = \frac{\gamma}{\mathcal{A}^2} + \varepsilon u_{i1} + \cdots\,, \quad y = \varepsilon^{-1}\left[x - x_i(\sigma)\right]\,, \quad \sigma = \varepsilon^2\mathcal{A}^2 t. \tag{3.27}$$

Here $\gamma = \gamma(\sigma)$ is to be found. Substituting (3.27) into (1.3), we get that $\nu_{i0} = \gamma^{-1}w(y)$, where $w(y) = \frac{3}{2}\text{sech}^2\left(\frac{y}{2}\right)$ satisfies (2.3). Defining $x_i' \equiv dx_i/d\sigma$, we get at next order on $-\infty < y < \infty$ that

$$\nu_{i1}'' - \nu_{i1} + 2w\nu_{i1} = -\gamma^{-2}w^2 u_{i1} - x_i'\gamma^{-1}w'\,, \quad \nu_{i1} \to 0 \quad \text{as} \quad |y| \to \infty\,, \tag{3.28a}$$

$$Du_{i1}'' - \gamma^{-1}w^2 = -\tau\varepsilon^3\mathcal{A}^2 x_i' u_{1i}'\,, \tag{3.28b}$$

To determine γ, we look for an outer solution as $u = u(x,\sigma)$. In this region we proceed as in §2 and replace $\varepsilon^{-1}u\nu^2 \to \gamma^{-1}\left(\int_{-\infty}^{\infty} w^2\,dy\right)\delta(x - x_i) = 6\gamma^{-1}\delta(x - x_i)$. This leads to the outer problem

$$Du_{xx} + (1 - u) - \frac{6}{\gamma}\sum_{i=0}^{1}\delta(x - x_i) = \varepsilon^2\mathcal{A}^2\tau u_\sigma\,, \tag{3.29}$$

with $u_x = 0$ at $x = \pm 1$. We conclude that the ODE (2.36c) remains valid in the intermediate regime only when we can asymptotically neglect the terms on the right hand sides of (3.28b) and (3.29). Assume that we can neglect the right hand side of (3.29). Then, the leading-order matching condition between the inner and outer solutions for u requires that $u(x_i) = 0$. This yields that

$$u = 1 - \frac{6}{\gamma}\sum_{i=0}^{1} G_0(x;x_i)\,, \qquad \gamma = 6\left(G_0(x_0;x_0) + G_0(x_1;x_0)\right)\,, \tag{3.30}$$

where the Green's function G_0 satisfies (2.8). The matching condition for u_{i1} is that $u_{i1}'(\pm\infty) = -6\gamma^{-1}\left(G_{0x}(x_{i\pm};x_i) + G_{0x}(x_i;x_j)\right)$. For $D \ll 1$, we use (2.8) to estimate $\gamma = O(D^{-1/2})$ and $u_{i1}'(\pm\infty) = O(D^{-1/2})$. Therefore, from (3.28b), it follows that we can neglect the u_t term in the core region when

$$\frac{\tau\varepsilon^2\mathcal{A}^2}{\sqrt{D}}\left(\frac{\varepsilon}{\sqrt{D}}\right) \ll 1\,. \tag{3.31}$$

Alternatively, using $\gamma = O(D^{-1/2})$ into (3.29), it follows that we can neglect the u_t term in (1.3) in the outer region when

$$\frac{\tau\varepsilon^2\mathcal{A}^2}{\sqrt{D}} \ll O(1)\,, \qquad \to \qquad \frac{\tau\varepsilon A^2}{\sqrt{D}} \ll O(1)\,, \tag{3.32}$$

where $A = \varepsilon^{1/2}\mathcal{A}$. Since $D \gg O(\varepsilon^2)$, (3.31) is satisfied when (3.32) holds.

This calculation shows that the dynamics (2.39b) and (2.36c) are valid in the intermediate regime only when τ satisfies (3.32). When $\tau = O(D^{1/2}\varepsilon^{-1}A^{-2})$, a traveling wave instability occurs as was discussed in §5 of [19] for perturbations of a one-spike equilibrium solution. Comparing the Hopf bifurcation threshold (3.26) with (3.32), we obtain an asymptotic threshold A_{sw} defined by

$$A_{sw} \equiv O\left[\left(\frac{\varepsilon}{\sqrt{D}}\right)^{1/6}\right]\,. \tag{3.33}$$

For the subregime $O\left(\varepsilon^{1/2}D^{-1/4}\right) \ll A \ll A_{sw}$, a Hopf bifurcation occurs before the onset of the traveling wave instability as τ is increased. Once the Hopf bifurcation occurs, the dynamics (2.39b) and (2.36c) are no longer valid. Alternatively, for the subregime $A_{sw} \ll A \ll O(1)$, the spike dynamics first become invalid as τ is increased as a result of a traveling wave instability.

Whenever $\tau < \tau_H$ and (3.32) both hold, the dynamics (2.39b) and (2.36c) describe the slow spike motion in the intermediate regime. Using the leading term $s_g \sim 4\left(\mathcal{A}/\mathcal{A}_{ke}\right)^2$ from (3.21), where $\mathcal{A}_{1e}$ and $\mathcal{A}_{2e}$ are given in (2.38) and (2.35), a simple calculation shows that (2.39b) and (2.36c) reduce to

$$\frac{dx_0}{dt} \sim -\frac{\varepsilon A^2}{6}\left[\tanh^2(\theta_0(1+x_0)) - \tanh^2(\theta_0(1-x_0))\right]\,, \quad \frac{d\alpha}{dt} \sim \frac{\varepsilon A^2}{6}\left[\tanh^2(\theta_0(1-\alpha)) - \tanh^2(\theta_0\alpha)\right]\,. \tag{3.34}$$

4 Numerical Experiments: Confirmation of the Theory

To validate the asymptotic theory, we now perform detailed numerical experiments on the GS model (1.3) and the GM model (1.4). The numerical results below are obtained using either the moving-mesh

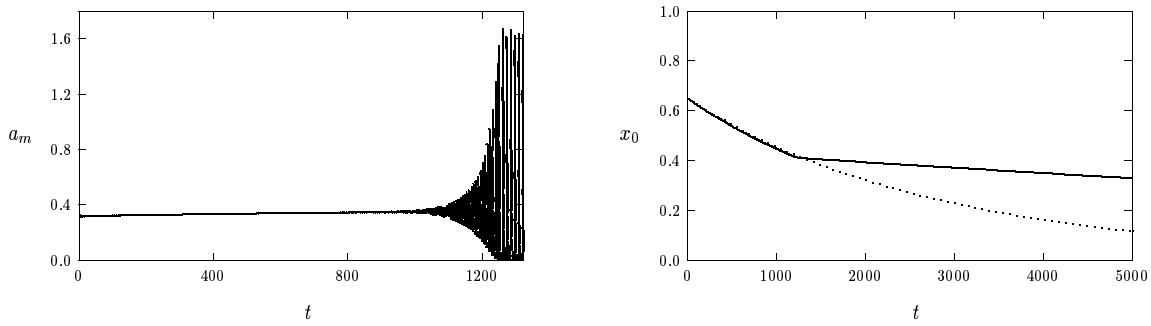

(a) a_m versus t

(b) x_0 versus t

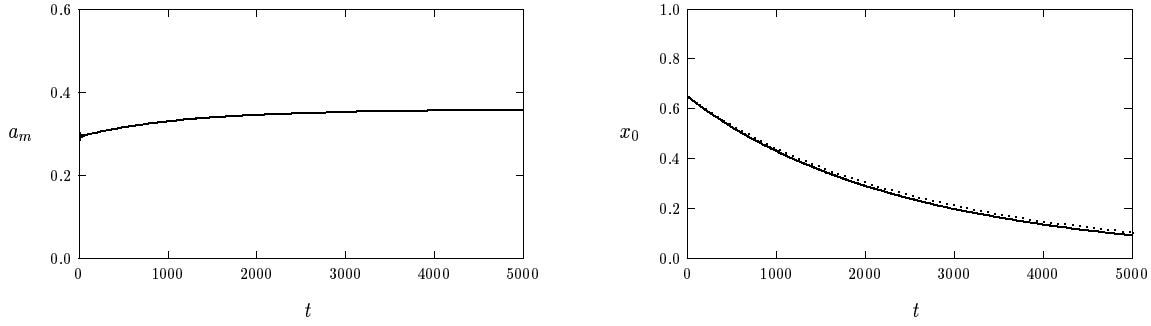

(c) a_m versus t

(d) x_0 versus t

Figure 8: **Experiment 1:** Top Row (Run 1): A one-spike solution for the GM model (1.4) with $\varepsilon = 0.02$, $D = 1.0$, $\tau = 1.4$, and $x_0(0) = 0.65$. The spike amplitude a_m (left figures) and location (right figures) versus t. The dotted and heavy solid curves are the dynamics (2.44b) and the full numerical result, respectively. Bottom row (Run 2): Same parameter values except that now $D = 0.75$.

method of [39] or the method-of-lines routine D03PCF of the NAG library [29]. In each experiment, the appropriate quasi-equilibrium solution in Principal Results 2.1–2.4 is taken as the initial condition. In addition, in the experiments below the Hopf bifurcation value of τ_H for the GM model or the GS model is obtained from the data used to generate Fig. 6 or Fig. 7, respectively.

Experiment 1: (GM model: One Spike) Consider a one-spike solution to the GM model (1.4) with $\varepsilon = 0.02$, $\tau = 1.4$, and the initial spike location $x_0(0) = 0.65$. For Run 1, we take $D = 1.0$. For this value, we obtain from Fig. 6(a) that a Hopf bifurcation occurs at $x_0 = 0.65$ when $\tau = \tau_H \approx 1.52$. Moreover, $\tau_H \approx 1.34$ when $x_0 = 0$. Therefore, the spike must pass through a zone of instability as it travels towards the origin. We compute that $\tau_H \approx 1.402$ when $x_0 = 0.475$. The resulting dynamic oscillatory instability, which is initiated at $t \approx 1.1 \times 10^3$, is shown in the top row of Fig. 8, where we observe that the asymptotic spike trajectory (2.44b) provides a close approximation to the true trajectory only before the instability is initiated.

In Run 2, we take the smaller value $D = 0.75$. From Fig. 6(a), we obtain that $\tau_H > \tau = 1.4$ for all $0 < x_0 < 0.65$. Therefore, we predict no dynamic oscillatory instabilities. This is shown in the bottom row of Fig. 8, where we observe that the spike drifts slowly towards the origin.

Experiment 2: (GM model: Two Spikes) Consider a two-spike solution to the GM model (1.4). For Run 1 we take $\varepsilon = 0.025$, $D = 0.75$, $\tau = 0.97$, and $x_1(0) = -x_0(0) = 0.75$. From Fig. 6(b) we have $\tau_H \approx 1.04$ when $x_1 = 0.75$ and that τ_H dips below 0.97 when $x_1 \approx 0.63$. Therefore, we predict that a dynamic oscillatory instability occurs before the rightmost spike reaches its equilibrium location at $x_1 = 0.5$. In Fig. 9(a) we show that the instability is initiated near $t \approx 600$ and that, as predicted by the theory of §3.3, the instability initially synchronizes the amplitudes of the two spikes. In this figure a_1 and a_2 are the (indistinguishable) amplitudes of the spikes located at x_0 and x_1, respectively. The small-scale oscillation develops into a large-scale sustained synchronous oscillation, which is ultimately broken at $t \approx 1.63 \times 10^3$ due to the amplification of small discretization errors (not shown). Near this time, the second spike, which was initially located at $x_1(0) = 0.75$, is annihilated. Since the parameters are such that they are below the instability threshold for a one-spike solution, the remaining spike is shown in Fig. 9(b) to drift slowly towards the origin without oscillation. In Fig. 9(b) we show a favorable comparison, up to the onset of the instability, between the full numerical result for the spike trajectory and the corresponding asymptotic result obtained from the ODE (2.42d).

For Run 2 we keep the same parameter values as in Run 1, except that we now decrease τ to $\tau = 0.9$. For this case, we find that $\tau < \tau_H$ for all x_1 with $0.5 < x_1 < 0.75$. Therefore, we predict no dynamic oscillatory instabilities. However, from Fig. 3(b), we predict that there will be a dynamic competition instability when $x_1 \approx 0.61$, which occurs before the spike reaches its equilibrium location at $x_1 \approx 0.5$. As shown in Fig. 10(a), this instability is initiated at $t \approx 820$ and leads to the annihilation of the second spike. Since the initial data is symmetric, the determination of the actual spike that gets annihilated is ultimately due to small discretization errors in the numerical method. After the second spike is destroyed, the remaining spike then travels to the origin as shown in Fig. 10(b).

For Run 3 we take the same parameter values as in Run 2, except that $D = 0.5$ is now smaller.

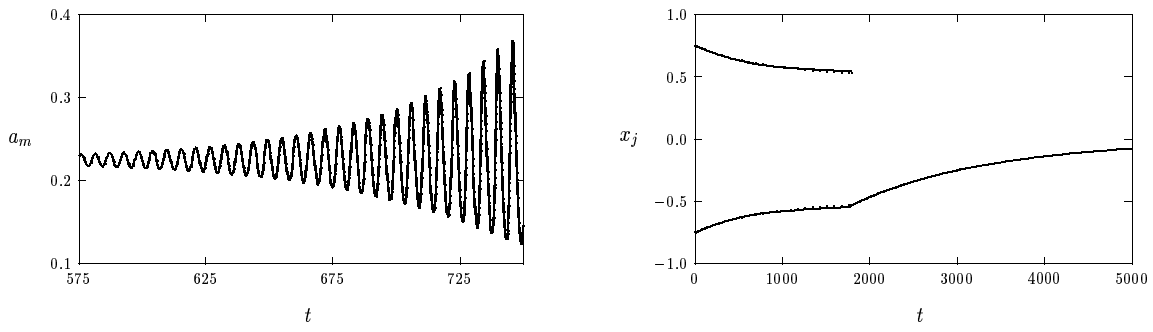

(a) a_m versus t (b) a_m versus t

Figure 9: **Experiment 2:** (Run 1): A two-spike solution for the GM model (1.4) with $\varepsilon = 0.025$, $D = 0.75$, $\tau = 0.97$, and $x_1(0) = -x_0(0) = 0.75$. Left figure: the spike amplitude a_1 (dotted curve) and a_2 (heavy solid curve) versus t showing the onset of a dynamic synchronous oscillatory instability. The amplitudes are indistinguishable in this plot. Right figure: the spike locations $x_j(t)$, for $j = 0, 1$. The heavy solid curve is the numerical result, and the dotted curves is the asymptotic result (2.42d).

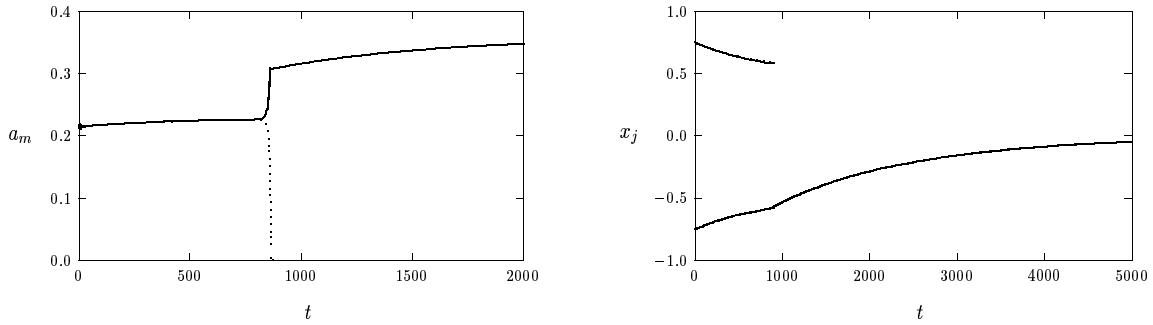

(a) a_m versus t (b) x_j versus t

Figure 10: **Experiment 2:** (Run 2): A two-spike solution for the GM model (1.4) with $\varepsilon = 0.025$, $D = 0.75$, $\tau = 0.9$, and $x_1(0) = -x_0(0) = 0.75$ showing a dynamic competition instability. Left figure: the spike amplitudes a_1 (heavy solid curve) and a_2 (dotted curve) versus t. Right figure: the asymptotic spike locations x_j from (2.42d) (dotted curves) and the full numerical results (heavy solid curve).

From Fig. 3(b) we predict that there are no dynamic competition instabilities. In Fig. 11 we plot the amplitude and the location of the spikes as they tend to $x_1 = -x_0 \to 1/2$ as $t \to \infty$. The asymptotic spike trajectory (2.42d) is shown to compare favorably with full numerical results.

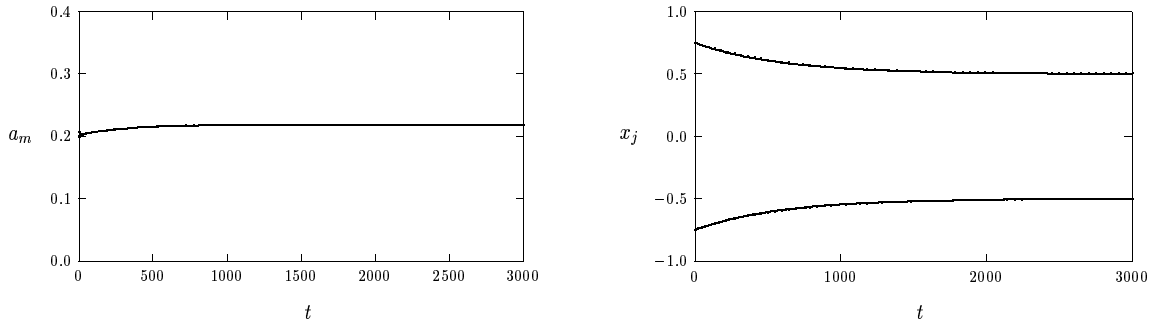

(a) a_m versus t (b) x_j versus t

Figure 11: **Experiment 2:** (Run 3): A two-spike solution for the GM model (1.4) with $\varepsilon = 0.025$, $D = 0.5$, $\tau = 0.9$, and $x_1(0) = -x_0(0) = 0.75$. For this parameter set there are no dynamic instabilities. Left figure: the spike amplitudes a_1 and a_2 trace out the same curve. Right figure: the asymptotic spike locations x_j from (2.42d) (dotted curves) and the full numerical results (heavy solid curve).

For Run 4 we take the same parameter values as in Run 3, except that now the initial data is taken to be slightly *asymmetric* by choosing the initial spike locations as $x_0(0) = -0.74$ and $x_1(0) = 0.75$. For this parameter set, we find from Fig. 12(a) and Fig. 12(b) that the spikes approach their equilibrium locations at $x_1 = -x_0 = 1/2$, but that a fast instability is triggered near $t = 1000$, which leads to the annihilation of the second spike. This type of instability, initially discovered in Example 4 of [15], occurs as a result of an instability associated with the small eigenvalues of order $\lambda = O(\varepsilon^2)$ in the spectrum of the linearization around the two-spike equilibrium solution at $x_1 = -x_0 = 1/2$. In Proposition 11 of [16], it was shown that there are two small eigenvalues for a two-spike equilibrium solution. These eigenvalues are asymptotically independent of τ when $\tau = O(1)$ and are real. For the GM model with $(p, q, m, s) = (2, 1, 2, 0)$, one of these eigenvalues is negative for all $D > 0$, while the other is negative only when $D < 0.3218$. Therefore, for $D = 0.5$, the equilibrium location is a saddle-point in phase-space with respect to the small eigenvalues. This weak instability then ultimately triggers a fast $O(1)$ dynamic competition instability in the two-spike profile, leading to the collapse of one of the spikes.

For Run 5 we take the same values as in Run 4, except that now D is decreased to $D = 0.3$. Since $D = 0.3 < 0.3218$, the two-spike equilibrium solution at $x_1 = -x_0 = 1/2$ is stable with respect to translations in the spike profile. In Fig. 13(a) and Fig. 13(a) we show that the spikes approach their equilibrium values without triggering any type of instability.

Experiment 3: (The Shadow GM Model) Consider a one-spike solution for the GM model (1.4)

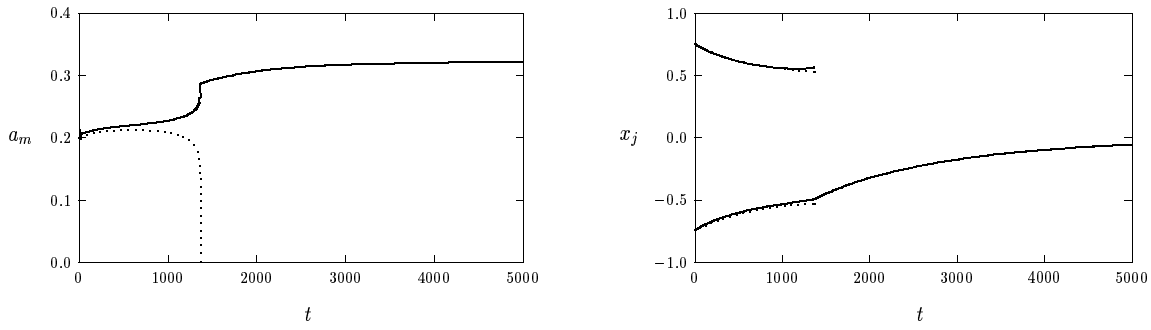

(a) a_m versus t (b) x_j versus t

Figure 12: **Experiment 2:** (Run 4): A two-spike solution for the GM model (1.4) with $\varepsilon = 0.025$, $D = 0.5$, $\tau = 0.9$, and slightly asymmetric data $x_1(0) = 0.75$, $x_0(0) = -0.74$. Left figure: the spike amplitudes a_1 (heavy solid curve) and a_2 (dotted curve) versus t. Right figure: the spike locations x_j from (2.42d) (dotted curves) for symmetric data and the full numerical results (heavy solid curve).

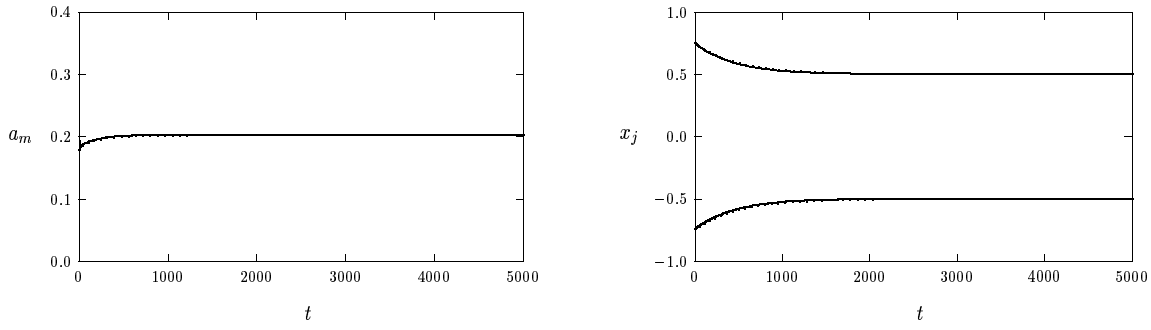

(a) a_m versus t (b) x_j versus t

Figure 13: **Experiment 2:** (Run 5): Same parameter values as in Fig. 12 where $\varepsilon = 0.025$, $\tau = 0.9$, $x_1(0) = 0.75$, $x_0(0) = -0.74$, except that now D is decreased to $D = 0.3$. For this value of D the equilibrium solution $x_1 = -x_0 = \frac{1}{2}$ is now stable with respect to the small eigenvalues of translation.

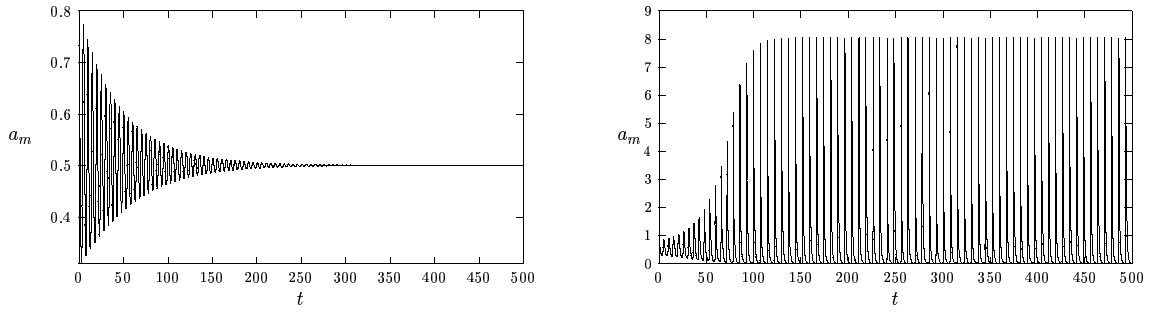

(a) $\tau = 0.75$ (b) $\tau = 0.80$

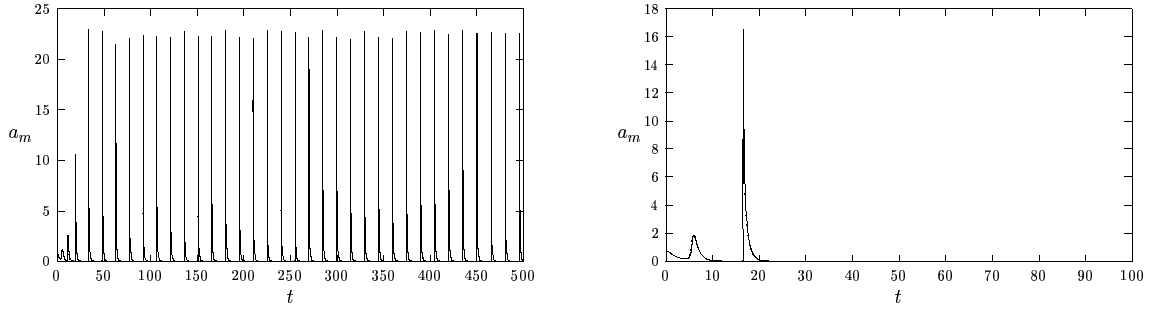

(c) $\tau = 0.95$ (d) $\tau = 1.1$

Figure 14: **Experiment 3:** The spike amplitude for a one-spike solution of the near-shadow GM model (1.4) with $\varepsilon = 0.025$, $D = 200$, and $x_0(0) = 0.0$. The figures correspond to four different values of τ.

where D is very large. For the shadow limit $D = \infty$, and for the exponent set $(p, q, m, s) = (2, 1, 2, 0)$, it is known from [43] that a Hopf bifurcation occurs when $\tau = \tau_H \approx 0.771$. For the values $\varepsilon = 0.02$, $D = 200$, and for a one-spike solution centered at the origin, in Fig. 14 we plot the spike amplitude versus t for four different values of τ. Notice that there is a sustained periodic oscillation when $\tau = 0.8$ and $\tau = 0.95$, and that the amplitude of this oscillation is very large when $\tau = 0.95$. As shown in [43], the zero solution is unstable when $\tau < 1$ and is stable when $\tau > 1$. We conjecture that the absence of the periodic solution in Fig. 14 for the value $\tau = 1.1$ is a result of the stability of the zero solution.

Experiment 4: (GS Model: One Spike) Consider a one-spike solution to the GS model (1.3). For Run 1 we take $\varepsilon = 0.015$, $D = 0.5$, $\mathcal{A} = 6.5$, $\tau = 12$, and $x_0(0) = 0.75$. From Fig. 7(a), the Hopf bifurcation value is $\tau_H \approx 13.5$ when $x_0 = 0.75$. In addition, $\tau_H > \tau = 12$ for any x_0 in $0 \le x_0 < 0.75$. Therefore, the spike should slowly travel to the origin under (2.39b) without experiencing any oscillatory instability. This is confirmed in Fig. 15 where it is shown that the asymptotic spike trajectory (2.39b)

provides a very close approximation to the true trajectory all the way to the origin.

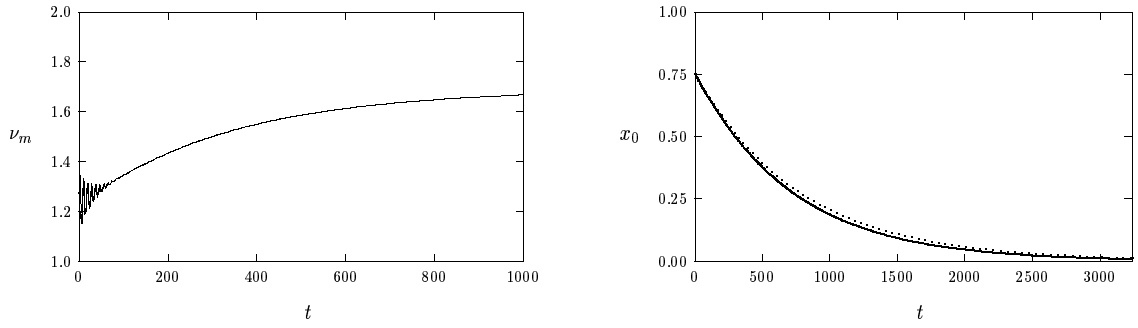

(a) ν_m versus t

(b) x_0 versus t

Figure 15: **Experiment 4:** (Run 1): A one-spike solution for the GS model (1.3) with $\varepsilon = 0.015$, $D = 0.5$, $\mathcal{A} = 6.5$, $\tau = 12$, and $x_0(0) = 0.75$. Left figure: the spike amplitude ν_m versus t. Right figure: the asymptotic dynamics from (2.39b) (dotted curve) and the full numerical results (heavy solid curve).

For Run 2 we take the same parameter values as in Run 1 except that now we increase τ to $\tau = 16.5$. Since $\tau > \tau_H \approx 13.5$, we expect a static oscillatory instability, since the instability is triggered at time $t = 0$. This is confirmed in Fig. 16 where we plot the spike amplitude $\nu_m \equiv \nu(x_0, t)$ versus t. In contrast to Experiment 1 (Run 1) showing a sustained dynamic oscillatory instability for a one-spike solution to the GM model (1.4), the oscillatory instability for the GS model (1.3) quickly leads to the collapse of the spike. This suggests that the GM model (1.4) has a supercritical Hopf bifurcation, whereas the bifurcation for the GS model (1.3) is subcritical.

In Run 3a we take $\varepsilon = 0.015$, $D = 2.5$, $\mathcal{A} = 6.5$, $\tau = 32.5$, and $x_0(0) = 0.85$. From Fig. 7(a), the Hopf bifurcation value is $\tau_H \approx 37.9$ when $x_0 = 0.85$. Therefore, since $\tau < \tau_H$ when $x_0 = 0.85$, the spike is stable at $t = 0$. On the interval $0 < x_0 < 0.85$, τ_H has a minimum value of $\tau_H \approx 30.8$ at $x_0 = 0.65$. Therefore, the spike must enter a zone of instability as it slowly drifts towards the origin. In Fig. 17(a) we show that the resulting dynamic oscillatory instability leads to the collapse of the spike. In Fig. 17(b) we show that the asymptotic dynamics (2.39b) closely approximates the true trajectory until the collapse occurs.

In Run 3b and Run 3c we take $\tau = 31.5$ and $\tau = 29$, respectively. The other parameter values are as in Run 3a. From Fig. 7(a) we conclude that $\tau = 29$ is below the Hopf bifurcation value for any $0 < x_0 < 0.85$. Alternatively, when $\tau = 31.5$, there is only a narrow zone near $x_0 = 0.65$ where $\tau > \tau_H$. In Fig. 18(a) we show that there is no oscillation in the spike amplitude when $\tau = 29$. However, for $\tau = 31.5$, a transient oscillation is initiated when the spike enters the thin unstable zone. This oscillation is extinguished as the spike leaves this zone and heads towards the origin. Similar types of safe passage through a thin unstable zone due to delayed bifurcation effects associated with slowly varying control

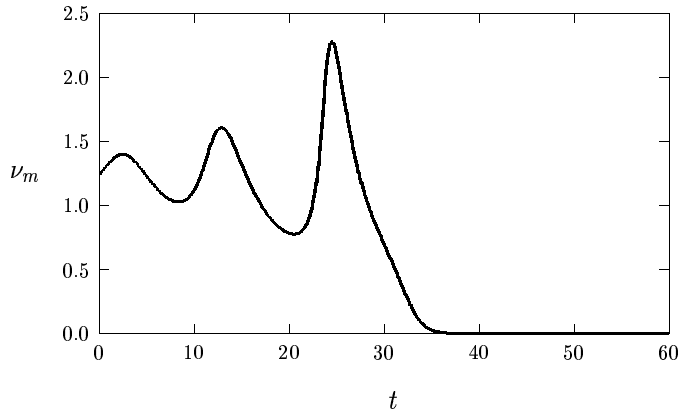

Figure 16: **Experiment 4:** (Run 2): The spike amplitude ν_m for a one-spike solution for the GS model (1.3) with $\varepsilon = 0.015$, $D = 0.5$, $\mathcal{A} = 6.5$, $\tau = 16.5$, and $x_0(0) = 0.75$. The spike is quickly annihilated in a static oscillatory instability.

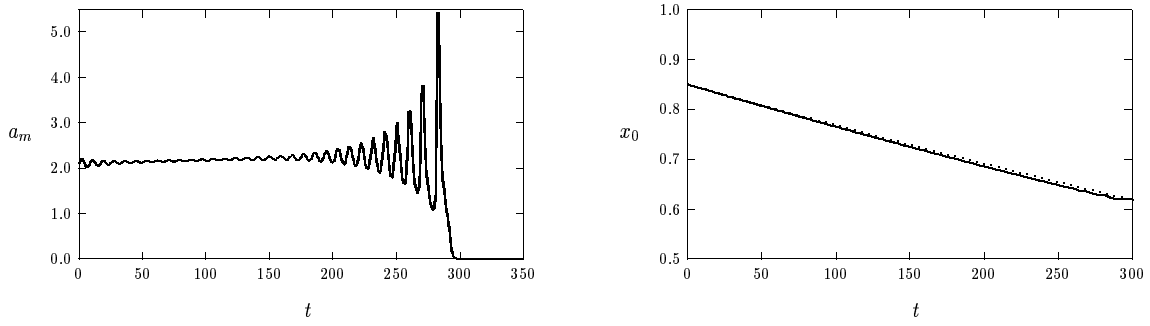

(a) ν_m versus t

(b) x_0 versus t

Figure 17: **Experiment 4:** (Run 3a): A one-spike solution for the GS model (1.3) with $\varepsilon = 0.015$, $D = 2.5$, $\mathcal{A} = 6.5$, $\tau = 32.5$, and $x_0(0) = 0.85$, showing a dynamic oscillatory instability. Left figure: the spike amplitude ν_m versus t. Right figure: the asymptotic dynamics (2.39b) (dotted curve) and the full numerical results (heavy solid curve).

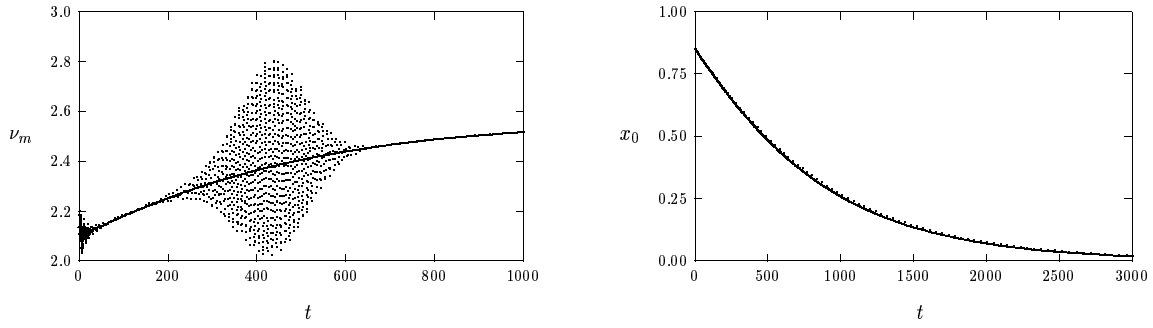

(a) ν_m versus t

(b) x_0 versus t

Figure 18: **Experiment 4:** (Run 3b,c): A one-spike solution for the GS model (1.3) with $\varepsilon = 0.015$, $D = 2.5$, $\mathcal{A} = 6.5$, and $x_0(0) = 0.85$. Left figure: the spike amplitude ν_m versus t for $\tau = 31.5$ (dotted curve) and $\tau = 29.0$ (heavy solid curve). Right figure: the asymptotic dynamics (2.39b) (dotted curve) and the full numerical results (heavy solid curve) for $\tau = 29$.

parameters is a well-known phenomena in ODE systems (cf. [10]). Its likely appearance here in a genuine PDE setting is novel. By decreasing ε, so that the spike travels more slowly through the unstable zone, we found that the transient oscillation could lead to a spike collapse event (not shown). In Fig. 18(b) we show a very favorable comparison between the asymptotic and numerical results for the spike trajectory when $\tau = 29$. Since the asymptotic dynamics (2.39b) is independent of τ, the plot of the spike trajectory when $\tau = 31.5$ is omitted since it is essentially indistinguishable from that when $\tau = 29$.

Experiment 5: (GS model: Two Spikes) Consider a two-spike solution to the GS model (1.3). For Run 1 we take $\varepsilon = 0.015$, $D = 0.75$, $\mathcal{A} = 6.5$, $\tau = 4.0$, and $\alpha(0) \equiv x_1(0) = -x_0(0) = 0.20$. From (3.15) of Proposition 3.7 and Fig. 4(a), we predict that there will be a competition instability whenever $\alpha(0) < \alpha_c \approx 0.3$. The resulting static competition instability, leading to the annihilation of the first spike ν_{m1} at $t \approx 130$, is shown in Fig. 19(a). In Fig. 19(b) we plot the numerical spike trajectories. After the first spike is annihilated, the second spike reverses direction and drifts slowly towards the origin.

For Run 2 we take the same parameter values as in Run 1 except that now we increase $\alpha(0)$ to $\alpha(0) = 0.33 > \alpha_c \approx 0.3$. Since $\alpha(0) > \alpha_c$ we predict no competition instabilities. Moreover, since $\tau < \tau_H$ on $.33 < \alpha < 0.5$, as seen from Fig. 7(b), we conclude that there are no oscillatory instabilities. In Fig. 20(a), where we show a favorable comparison between the asymptotic spike dynamics (2.36c) and corresponding full numerical spike trajectories, we indeed confirm that the spikes slowly drift towards their equilibrium locations without triggering any instabilities.

For Run 3, we take the same values $\alpha(0) = 0.33$, $\varepsilon = 0.015$, $\mathcal{A} = 6.5$, and $D = 0.75$, as in Run 2, but we now increase τ to $\tau = 7.0$. From Fig. 7(b), we find that $\tau_H \approx 6.7$ when $\alpha = 0.33$. Therefore, since $\tau > \tau_H$ at $t = 0$, we expect an oscillatory instability to be triggered at $t = 0$. From §3.3, we predict

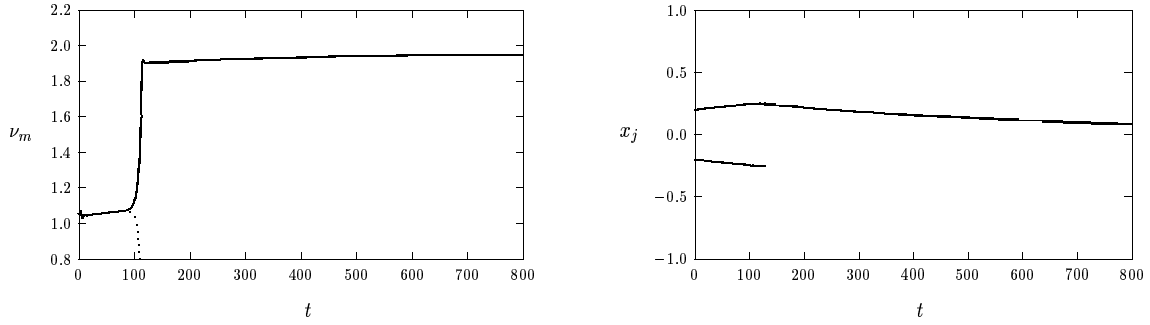

(a) ν_m versus t (b) x_j versus t

Figure 19: **Experiment 5:** (Run 1): A two-spike solution for the GS model (1.3) with $\varepsilon = 0.015$, $D = 0.75$, $\mathcal{A} = 6.5$, $\tau = 4.0$ and $x_1(0) = -x_0(0) = 0.20$. Left figure: the spike amplitudes ν_1 (dotted curve) and ν_2 (heavy solid curve) versus t. Right figure: the numerical spike trajectories versus t. After the collapse of the first spike, the surviving spike reverses direction and drifts slowly towards the origin.

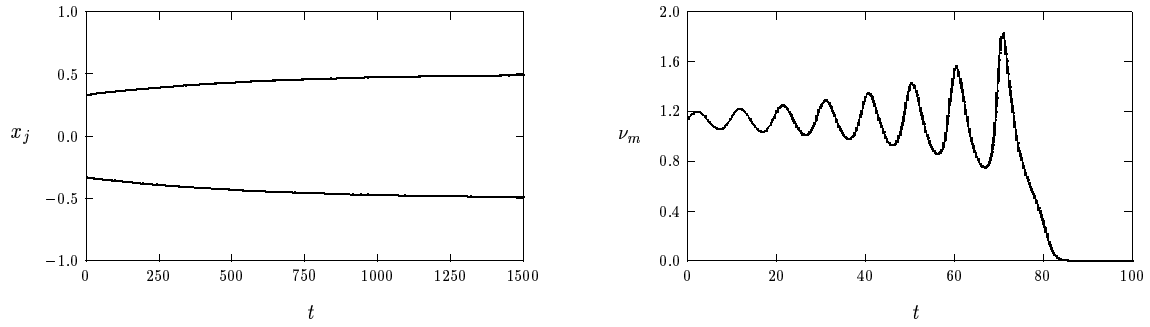

(a) x_j versus t (b) ν_m versus t

Figure 20: **Experiment 5:** (Run 2,3): Two-spike solutions for the GS model (1.3). Left figure (Run 2): the asymptotic spike dynamics (2.36c) (dotted curves) and numerical spike trajectories (heavy solid curves) when $\varepsilon = 0.015$, $D = 0.75$, $\mathcal{A} = 6.5$, $\tau = 4.0$, and $\alpha(0) = 0.33$. Right figure (Run 3): a static synchronous oscillatory instability in the spike amplitudes ν_1 and ν_2 for $\varepsilon = 0.015$, $D = 0.75$, $\mathcal{A} = 6.5$, $\tau = 7.0$, and $\alpha(0) = 0.33$.

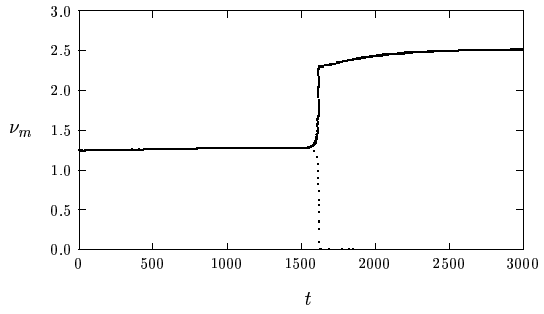

(a) Run 4: ν_m versus t

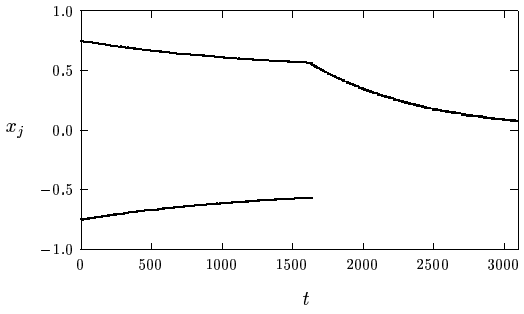

(b) Run 4: x_j versus t

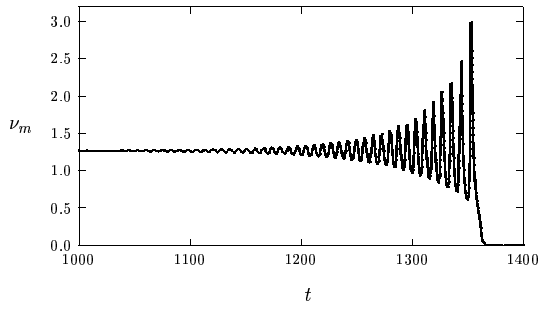

(c) Run 5: ν_m versus t

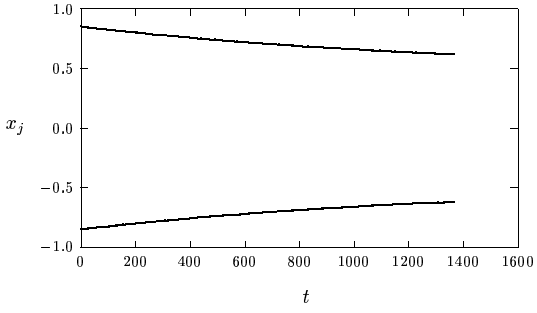

(d) Run 5: x_j versus t

Figure 21: **Experiment 5:** (Run 4,5). Two-spike solutions to the GS model (1.3). Top row (Run 4): the spike amplitudes ν_1 (dotted) and ν_2 (heavy solid), and the asymptotic (dotted) and full numerical (heavy solid) spike trajectories for $\varepsilon = 0.015$, $D = 2.25$, $\mathcal{A} = 6.5$, $\tau = 4.0$, and $\alpha(0) = 0.75$. Bottom row (Run 5): same plots but now for $\varepsilon = 0.015$, $D = 2.25$, $\mathcal{A} = 6.5$, $\tau = 5.3$, and $\alpha(0) = 0.85$.

that the resulting static oscillatory instability should synchronize the amplitudes of the two spikes near the onset of the instability. This is confirmed in Fig. 20(b). Away from onset, the instability is shown to lead to the oscillatory collapse of both spikes.

In Run 4 and Run 5 we show the possibility of either a dynamic competition instability or a dynamic oscillatory instability for symmetric spikes whose inter-separation distance is slowly decreasing in time. For both runs we take $\varepsilon = 0.015$, $D = 2.25$, and $\mathcal{A} = 6.5$.

For Run 4 we choose $\tau = 4.0$ and $\alpha(0) = 0.75$. From (3.15) and Fig. 4(a), we conclude that there is a dynamic competition instability when $\alpha < \alpha_c \approx 0.6$. Therefore, this instability will be triggered before the spikes reach their equilibrium locations at ± 0.5. In Fig. 21(a) we show that this instability leads to the annihilation of the first spike at $t \approx 1630$. The surviving spike then drifts towards the origin. In Fig. 21(b) we show that the asymptotic spike dynamics (2.36c) and the full numerical spike

trajectories are essentially indistinguishable before the collapse event. After the collapse time, the asymptotic two-spike dynamics (2.36c) is invalid and we only plot the numerical result.

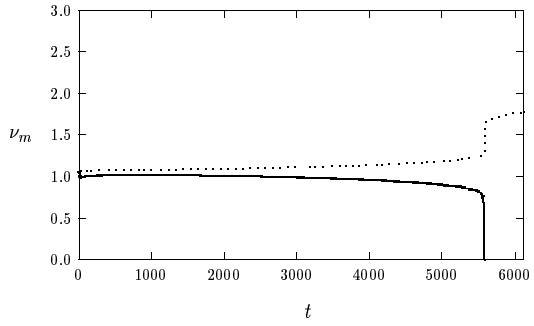

(a) ν_m versus t

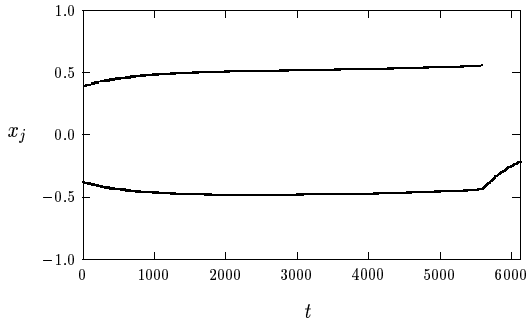

(b) x_j versus t

Figure 22: **Experiment 5:** (Run 6): Two-spike evolutions for the GS model (1.3) that are slightly asymmetric at $t = 0$. The parameter values are $\varepsilon = 0.015$, $D = 0.75$, $\mathcal{A} = 6.1$, $\tau = 4.0$, and the initial spike locations are $x_0(0) = -0.38$, and $x_1(0) = 0.39$. Left figure: the spike amplitudes ν_1 (dotted curve) and ν_2 (heavy solid curve). Right figure: the numerical spike trajectories.

For Run 5 we take $\tau = 5.3$, and $\alpha(0) = 0.85$. From Fig. 7(b) we conclude that $\tau_H \approx 6.0$ when $\alpha(0) = 0.85$. In addition, $\tau_H \approx 5.3$ when $\alpha = 0.7$, and $\tau_H < 5.3$ on $0.5 < \alpha < 0.7$. Therefore, for this larger value of τ, the spikes are initially stable, but they will experience a dynamic oscillatory instability when $\alpha \approx 0.7$. Notice that this occurs *before* the onset of the competition instability at $\alpha = 0.6$ in Run 4. The dynamic oscillatory instability is clearly seen in Fig. 21(c), where we show that both spikes are annihilated in a synchronous oscillatory collapse when $t \approx 1360$ for $\alpha \approx 0.63$. The observation that the spikes are annihilated at some point strictly inside the unstable zone is probably a result of a delayed bifurcation effect due to the slow drift of the spikes. Once again, as shown in Fig. 21(d), there is a very favorable comparison between the asymptotic spike dynamics (2.36c) and the full numerical spike trajectories before the collapse event.

Finally, in Run 6 we take $\varepsilon = 0.015$, $D = 0.75$, $\mathcal{A} = 6.1$, and $\tau = 4.0$. The initial locations of the spikes are slightly asymmetric, with $x_0(0) = -0.38$ and $x_1(0) = 0.39$, so that the asymptotic spike dynamics (2.36c) is not relevant. The spike dynamics in this case is similar to that shown in Experiment 2 (Run 4) for a two-spike solution to the GM model (1.4). In Proposition 3.4 of [19], and for $\tau = O(1)$, it was shown that the two small eigenvalues associated with a two-spike equilibrium solution are both negative if and only if $\mathcal{A} > \mathcal{A}_{2S}$, where $\mathcal{A}_{2S} \equiv \mathcal{A}_{2e} \coth(D^{-1/2})$. Alternatively, one small eigenvalue is positive and the other is negative when $\mathcal{A}$ satisfies $\mathcal{A}_{2e} < \mathcal{A} < \mathcal{A}_{2S}$. For $D = 0.75$, we calculate $\mathcal{A}_{2S} = 6.296$. Therefore, for $\mathcal{A} = 6.1$, it follows that the equilibrium locations at ± 0.5 are a saddle-point in phase-space with respect to the translation instabilities associated with the small eigenvalues. The

slight asymmetry in the initial data leads to a slow approach towards this saddle point along a trajectory that is close to the stable manifold of the saddle. By calculating the unstable eigenfunction in [19], it was shown that this stable manifold locally represents the symmetric two-spike quasi-equilibrium solution. As t increases, the trajectories depart rapidly from the stable manifold. This ultimately leads to the triggering of an instability associated with the large eigenvalues. In Fig. 22(a) we show that a dynamic competition instability results, which then leads to the collapse of one spike. The surviving spike is seen to drift slowly towards the origin. As a remark, if we repeat this experiment with $\mathcal{A} = 6.5 > \mathcal{A}_{2S}$, for which the two-spike equilibrium is now stable with respect to translations, the two slightly asymmetric spikes will tend to their equilibrium locations at ± 0.5 as t increases (not shown).

5 The Infinite-Line Problem

In §5.1 we give some results for the dynamics and stability of two-spike quasi-equilibrium solutions to the GS and GM models on the infinite line. We carefully illustrate our new contributions to the study of this problem. In §5.2 and Appendix A we compare our results with those of [2], [3], [6], and [9].

5.1 The Stability and Dynamics of Two-Spike Quasi-Equilibria

The infinite-line problem for the GS model is to seek spike solutions for (1.3) on $-\infty < x < \infty$. Without loss of generality we can set $D = 1$ in (1.3). This leads to the following problem for ν_i and u_i:

$$\nu_{it} = \varepsilon_i^2 \nu_{ixx} - \nu_i + \mathcal{A}_i u_i \nu_i^2 \,, \qquad \tau u_{it} = u_{ixx} + (1 - u_i) - \varepsilon_i^{-1} u_i \nu_i^2 \,. \tag{5.1}$$

Consider a two-spike quasi-equilibrium solution to (5.1) with spikes located at $\alpha_i \equiv x_1 = -x_0 \gg O(\varepsilon_i)$. To derive an ODE for α_i, and to analyze the stability of the solution, we can proceed as in §2 by replacing the finite-domain Green's functions (2.8) and (2.26) with their infinite-line counterparts, satisfying

$$G_{0xx} - G_0 = -\delta(x - \xi)\,; \quad G_{\lambda xx} - (1 + \tau\lambda) G_\lambda = -\delta(x - \xi)\,; \qquad G_0\,,\, G_\lambda \to 0\,, \quad |x| \to \infty\,. \tag{5.2}$$

However, a simpler way to derive results for (5.1) is to take the limit $D \to 0$, or equivalently $\theta_0 \equiv D^{-1/2} \to \infty$, in the GS results of §2 and §3 while keeping the product $\theta_0 \alpha$ given there fixed. A simple scaling argument between (1.3) and (5.1) gives the following correspondence between the infinite-line variables ν_i, u_i, $\mathcal{A}_i$, ε_i, and α_i, and their finite-domain counterparts ν, u, $\mathcal{A}$, ε, and α:

$$\mathcal{A}_i = D^{1/4} \mathcal{A}\,, \qquad \nu_i = D^{-1/4} \nu\,, \qquad u_i = u\,, \qquad \varepsilon_i = \varepsilon D^{-1/2}\,, \qquad \alpha_i = \alpha D^{-1/2}\,. \tag{5.3}$$

Therefore, in Principal Result 2.1, we use (5.3) and then take the limit $D \to 0$ with fixed $\alpha_i \equiv \alpha D^{-1/2}$. In this way, we obtain the following result for two-spike quasi-equilibrium solutions of (5.1):

Principal Result 5.1: *Let $\varepsilon_i \ll 1$, $\tau = O(1)$, and consider a quasi-equilibrium two-spike solution for the GS model (5.1) with spikes located at $\alpha_i \equiv x_1 = -x_0 > 0$. Suppose that $\mathcal{A}_i > \mathcal{A}_{2e}^\infty$, where*

$$\mathcal{A}_{2e}^\infty = \sqrt{12}\left(1 + e^{-2\alpha_i}\right)^{1/2}\,, \tag{5.4}$$

and that this solution is stable on an $O(1)$ time-scale. Then, the dynamics of α_i is given by

$$\frac{d\alpha_i}{dt} \sim \frac{2\varepsilon_i^2 s_g e^{-2\alpha_i}}{1+e^{-2\alpha_i}}\,, \qquad s_g = 2\left[1 \pm \sqrt{1-\left(\frac{\mathcal{A}_{2e}^{\infty}}{\mathcal{A}_i}\right)^2}\right]^{-1} - 1\,. \tag{5.5}$$

The stability of this solution is determined by the spectrum of the NLEP (3.1), or equivalently (3.3), where the multiplier $\chi = C^{-1}$ is given by

$$C_{gs\pm}^{\infty} \equiv \left[\chi_{gs\pm}^{\infty}\right]^{-1} \equiv \frac{1}{2} + \frac{\sqrt{1+\tau\lambda}}{2s_g}\left(\frac{1+e^{-2\alpha_i}}{1 \pm e^{-2\alpha_i\sqrt{1+\tau\lambda}}}\right)\,. \tag{5.6}$$

The corresponding localized eigenfunction has the form given in (2.37c).

The dynamics (5.5) is equivalent to equation (4.19) of §4.2 of [3] (see Appendix A). However, the stability of the quasi-equilibrium solution in this regime was not studied in [2] and [3]. Therefore, the NLEP (5.6) is a new result. To determine the parameter range where there are competition instabilities, we let $D \to 0$ with $\alpha_i \equiv \theta_0 \alpha$ fixed in Proposition 3.7. This leads to the next result.

Proposition 5.2: *The two-spike quasi-equilibrium solution for the infinite-line GS model (5.1) is unstable when $0 < s_g < 1$. Alternatively, for the minus root in (5.5) where $s_g > 1$, and for $0 \le \tau < \tau_H$ for some $\tau_H > 0$, the quasi-equilibrium solution is unstable as a result of a unique real eigenvalue in $Re(\lambda) > 0$ whenever $\mathcal{A}_i$ satisfies $\mathcal{A}_{2e}^{\infty} < \mathcal{A}_i < \mathcal{A}_{2L}^{\infty}$, where*

$$\mathcal{A}_{2L}^{\infty} \equiv \mathcal{A}_{2e}^{\infty}\frac{[1+\coth(\alpha_i)]}{2\sqrt{\coth(\alpha_i)}}\,. \tag{5.7}$$

Here $\mathcal{A}_{2e}^{\infty}$ is given in (5.4). Alternatively, for $0 < \tau < \tau_H$, the solution is stable when $\mathcal{A}_i > \mathcal{A}_{2L}^{\infty}$.

The thresholds $\mathcal{A}_{2e}^{\infty}$ and $\mathcal{A}_{2L}^{\infty}$ are monotone decreasing functions of α_i with $\mathcal{A}_{2L}^{\infty} - \mathcal{A}_{2e}^{\infty} \to 0^+$ as $\alpha_i \to \infty$. Proposition 5.2 predicts that a competition instability occurs at $t = 0$ when $\mathcal{A}_i$ satisfies $\mathcal{A}_{2e}^{\infty} < \mathcal{A}_i < \mathcal{A}_{2L}^{\infty}$ for the initial value $\alpha_i(0)$. Setting $\mathcal{A}_i = \mathcal{A}_{2L}^{\infty}$ in (5.7), we define a critical distance by

$$\alpha_{ic} \equiv \frac{1}{2}\log\left(\frac{s_g+1}{s_g-1}\right)\,, \quad s_g = 2\left[1 - \sqrt{1-\left(\frac{\mathcal{A}_{2e}^{\infty}}{\mathcal{A}_i}\right)^2}\right]^{-1} - 1\,. \tag{5.8}$$

For a fixed $\mathcal{A}_i$ with $\mathcal{A}_i > \mathcal{A}_{2e}^{\infty}$, a competition instability occurs at time $t = 0$ if the initial spike separation distance $2\alpha_i(0)$ is too small in the sense that $0 < \alpha_i(0) < \alpha_{ic}$. However, since (5.5) yields $\alpha_i'(t) > 0$ and since $\mathcal{A}_{2L}^{\infty}$ is monotone decreasing in α_i, we conclude, in contrast to the finite-domain problem, that there are no dynamic competition instabilities for the infinite-line problem.

Next, we determine the Hopf bifurcation value τ_H as a function of α_i for various $\mathcal{A}_i$ from the numerical solution to the NLEP (3.1) with multiplier (5.6). As in §3.3, we define $\tau_H \equiv \min(\tau_{H+}, \tau_{H-})$, where $\tau_{H\pm}$ are the Hopf bifurcation values for $C_{gs\pm}^{\infty}$, and we find numerically that the minimum is set by C_{gs+}^{∞}. From (2.37c), this corresponds to a synchronous oscillatory instability. In Fig. 23(a) and Fig. 23(b) we plot τ_H for large and small values of $\mathcal{A}$, respectively. For the larger values of $\mathcal{A}$ given in Fig. 23(a) we show a favorable comparison between the scaling law (5.12), given below, and the full

numerical results. From the analysis above, there is a competition instability for any α_i in $0 < \alpha_i < \alpha_{ic}$ and so, on this range, we have instability for *any* $\tau > 0$. Alternatively, for $\alpha_i > \alpha_{ic}$, we have instability only when $\tau > \tau_H = \tau_{H+}$. Therefore, in Fig. 23(a) and Fig. 23(b), we only consider $\alpha_i > \alpha_{ic}$. For the values of $\mathcal{A}_i$ in these figures we calculate the following pairs of $(\mathcal{A}_i, \alpha_{ic})$:

$$(7.0, 0.14)\,, \quad (6.0, 0.20)\,, \quad (5.0, 0.33)\,, \quad (4.5, 0.45)\,, \quad (4.0, 0.69)\,, \quad (3.75, 0.96)\,, \quad (3.5, 1.95)\,. \tag{5.9}$$

As $\alpha_i \to \alpha_{ic}^+$, the Hopf bifurcation frequency, λ_{I-}, for C_{gs-} tends to zero. Thus, τ_{H-} is not defined for $\alpha_i < \alpha_{ic}$. Similarly, τ_{H+} is not defined on the range $\mathcal{A}_i < \mathcal{A}_{2e}^{\infty}$. Therefore, the curves in Fig. 23(b) terminate below some critical of α where there is non-existence of two-spike quasi-equilibria. Since our numerical evidence suggests that τ_H is an increasing function of α_i, we conclude, in contrast to the finite-domain problem, that there are no dynamic oscillatory instabilities for the infinite-line problem.

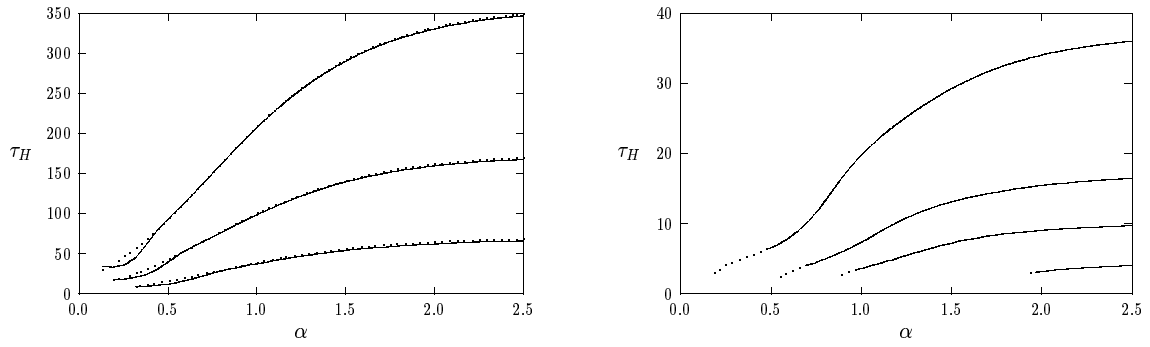

(a) τ_H: large $\mathcal{A}_i$ (b) τ_H: small $\mathcal{A}_i$

Figure 23: The Hopf bifurcation value τ_H versus α_i for the multiplier (5.6). Left figure: plots on the range $\alpha_i > \alpha_{ic}$ for $\mathcal{A}_i = 7.0$ (top curve), $\mathcal{A}_i = 6.0$ (middle curve), and $\mathcal{A}_i = 5.0$ (bottom curve). The dotted lines are the scaling law (5.12) (indistinguishable). Right figure: from top to bottom, plots are for $\mathcal{A}_i = 4.5$, $\mathcal{A}_i = 4.0$, $\mathcal{A}_i = 3.75$, and $\mathcal{A}_i = 3.5$. The dotted portions of these curves are for $\alpha_i < \alpha_{ic}$.

Next, we consider the intermediate regime for (5.1), defined by $O(\varepsilon_i^{1/2}) \ll A_i \ll O(1)$, where A_i is defined by $A_i \equiv \varepsilon^{1/2}\mathcal{A}_i$. In this regime, we have $s_g \gg 1$, so that $\alpha_{ic} \sim s_g^{-1}$ from (5.8). Therefore, using $s_g \sim 4\,(\mathcal{A}_i/\mathcal{A}_{2e}^{\infty})^2 - 2 + o(1)$ from (5.5) together with (5.4) for $\mathcal{A}_{2e}^{\infty}$, a simple calculation shows that we have competition instabilities only when $0 < \alpha_i < \alpha_{ic}$, where

$$\alpha_{ic} \sim \frac{3\varepsilon}{A_i^2}\,, \qquad O(\varepsilon_i^{1/2}) \ll A_i \ll O(1)\,. \tag{5.10}$$

Since $O(\varepsilon_i) < \alpha_{ic} \ll O(1)$, the interval in α_i where competition instabilities occur in this regime is very narrow. This is a new result. In this regime a scaling law for the Hopf bifurcation value τ_H can be

derived. Letting $s_g \gg 1$ in (5.6), a Hopf bifurcation can only occur if $\tau \gg 1$. For $\tau \gg 1$, (5.6) becomes

$$C_{gs\pm}^{\infty} \sim \frac{1}{2} + \frac{\sqrt{\tau\lambda}}{2s_g}\left(1 + e^{-2\alpha_i}\right) . \tag{5.11}$$

Then, we let $\tau = \tau_0 s_g^2/\left(1+e^{-2\alpha_i}\right)^2$, to get that $C_{gs\pm}^{\infty}$ tends to a common limiting multiplier $C_{gs\pm}^{\infty} \sim \frac{1}{2}\left(1+\sqrt{\tau_0\lambda}\right)$. This observation is explored further in §5.2. With this limiting multiplier, the corresponding NLEP has a Hopf bifurcation at $\tau_{0H} = 1.748$ (see [4] or §4 of [17]). Therefore, using $s_g \sim 4\left(\mathcal{A}_i/\mathcal{A}_{2e}^{\infty}\right)^2 - 2 + o(1)$, and (5.4) for $\mathcal{A}_{2e}^{\infty}$, we obtain the scaling law

$$\tau_H \sim \frac{(0.194)\varepsilon_i^{-2}A_i^4}{\left(1+e^{-2\alpha_i}\right)^4}\left(1 - \frac{6\varepsilon_i\left(1+e^{-2\alpha_i}\right)}{A_i^2}\right)^2 + o(1)\,, \qquad O(\varepsilon_i^{1/2}) \ll A_i \ll O(1)\,. \tag{5.12}$$

Since τ_H is a monotonically increasing function of α_i, there are no dynamic oscillatory instabilities in this regime. Finally, assuming that $\tau\varepsilon_i A_i^2 \ll 1$ (recall (3.32)) and $\tau < \tau_H$, the ODE (5.5) remains valid in this regime. Using the leading term $s_g \sim 4\left(\mathcal{A}_i/\mathcal{A}_{2e}^{\infty}\right)^2$ and (5.4) for $\mathcal{A}_{2e}^{\infty}$, (5.5) reduces to

$$\frac{d\alpha}{dt} \sim \frac{2\varepsilon_i A_i^2}{3}\frac{e^{-2\alpha_i}}{\left(1+e^{-2\alpha_i}\right)^2}\,, \qquad O(\varepsilon_i^{1/2}) \ll A_i \ll O(1)\,. \tag{5.13}$$

The ODE (5.13) and the leading term in the stability threshold (5.12), obtained by neglecting the correction term in the large bracket in (5.12), were obtained previously in [2] (see Appendix A).

Next, we consider the infinite-line GM model (1.4) with exponent set $(p,q,m,s) = (2,1,2,0)$, where

$$a_{it} = \varepsilon_i^2 a_{ixx} - a_i + \frac{a_i^2}{h_i}\,, \qquad \tau h_{it} = h_{ixx} - h_i + \varepsilon_i^{-1}a_i^2\,. \tag{5.14}$$

On the infinite line, we can $D = 1$ in (1.4) without loss of generality. As for the GS model, a simple way to analyze (5.14) is to take the limit $D \to 0$ in the GM results of §2 and §3 while keeping the product $\alpha D^{-1/2}$ fixed. The scaling relationship between the infinite-line variables a_i, h_i, ε_i, and α_i, for (5.14) and their finite-domain counterparts a, h, ε, and α, for (1.4) is

$$a_i = D^{-1/2}a\,, \qquad h_i = D^{-1/2}h\,, \qquad \varepsilon_i = \varepsilon D^{-1/2}\,, \qquad \alpha_i = \alpha D^{-1/2}\,. \tag{5.15}$$

The next result arises by letting $D \to 0$, with fixed α_i, in Principal Result 2.3 and by using (5.15).

Principal Result 5.3: *Let $\varepsilon_i \ll 1$, $\tau = O(1)$, and consider a two-spike quasi-equilibrium solution for the GM model (5.14) with spikes located at $\alpha_i \equiv x_1 = -x_0 > 0$. Assuming that this solution is stable, the dynamics of α_i is given by*

$$\frac{d\alpha_i}{dt} \sim \frac{2\varepsilon_i^2 e^{-2\alpha_i}}{1+e^{-2\alpha_i}}\,. \tag{5.16}$$

The corresponding NLEP governing the stability of this solution is given by (3.1), with the multiplier

$$C_{gm\pm}^{\infty} \equiv \left[\chi_{gm\pm}^{\infty}\right]^{-1} \equiv \frac{\sqrt{1+\tau\lambda}}{2}\left(\frac{1+e^{-2\alpha_i}}{1 \pm e^{-2\alpha_i\sqrt{1+\tau\lambda}}}\right)\,. \tag{5.17}$$

The corresponding localized eigenfunction has the form given in (2.37c).

The dynamics (5.16) was obtained from (2.42d) by taking the limit $D \to 0$ with $\alpha D^{-1/2}$ fixed. As stated in §2, (2.42d) was first derived in equation (5.3) of Corollary 5.2 of [15]. As remarked in §5.2, the dynamics (5.16) is also equivalent to equation (5.6) of [9]. However, the NLEP problem (3.1) with multiplier given in (5.17) is a new result.

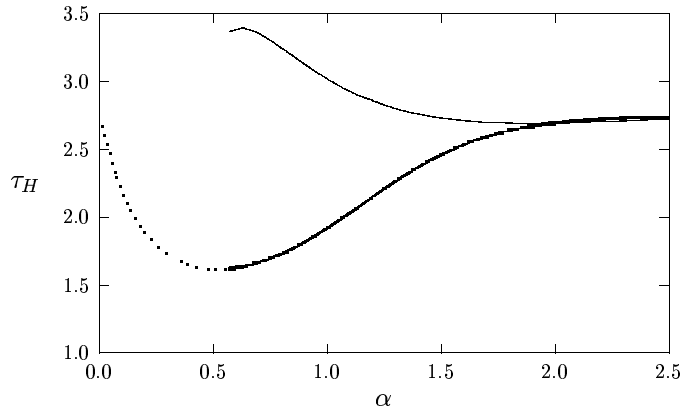

Figure 24: Plot of τ_{H+} (heavy solid curve) and τ_{H-} (solid curve) versus α_i for the GM model (5.14). The dotted curve is τ_{H+} for $\alpha_i < \alpha_{ic}$ where there is a competition instability for any $\tau > 0$.

To determine the parameter range where there are competition instabilities we let $D \to 0$, with $\alpha_i \equiv \alpha D^{-1/2}$ fixed, in (3.12) of Proposition 3.6 of §3.2. This yields the critical distance $\alpha_{ic} \equiv \frac{1}{2}\log 3$. Therefore, for any initial value $\alpha_i(0)$ with $0 < \alpha_i(0) < \alpha_{ic}$, there is a competition instability at time $t = 0$. However, there are no dynamic competition instabilities when $\alpha_i(0) > \alpha_{ic}$, since $\alpha_i' > 0$ under (5.16) ensures that $\alpha_i(t) > \alpha_{ic}$ for all $t > 0$. To study oscillatory instabilities, we numerically compute the Hopf bifurcation threshold $\tau = \tau_H = \min(\tau_{H+}, \tau_{H-})$, where $\tau_{H\pm}$ are the Hopf bifurcation values for $C^{\infty}_{gm\pm}$. The results for $\tau_{H\pm}$ versus α_i, plotted in Fig. 24, show that the minimum is again set by C^{∞}_{gm+}, which corresponds to a synchronous oscillatory instability from (2.37c). Notice that τ_{H-} is only defined for $\alpha_i > \alpha_{ic}$, corresponding to the range where $C^{\infty}_{gm-}(0) < 1$. As $\alpha_i \to \alpha_{ic}^{+}$ the imaginary part λ_I of the eigenvalue for the Hopf bifurcation associated with C^{∞}_{gm-} tends to zero. The numerical evidence shown in Fig. 24 suggests that τ_H has its minimum at $\alpha_i = \alpha_{ic} \equiv \frac{1}{2}\log 3 \approx 0.549$, and that τ_H is increasing for $\alpha_i > \alpha_{ic}$. Therefore, since $\alpha_i'(t) > 0$ under (5.16), we conclude that whenever the initial state satisfies $\alpha_i(0) > \alpha_{ic}$ and $\tau < \tau_H$, the two-spike quasi-equilibrium solution will be stable at all later times. Hence, there are no dynamic oscillatory instabilities for the infinite-line GM model.

5.2 Other Infinite-Line Results

We now make some general remarks on equivalence principles between the GS and GM models, and we discuss some previous work for the infinite-line problem. In [6] a rigorous analysis was given for the

existence and stability of a one-spike solution to the following infinite-line GM model:

$$V_T = \delta^2 V_{XX} - V + U^{\alpha_2} V^{\beta_2} \gamma_2 \,, \qquad \delta^2 U_T = U_{XX} - \delta^2 \mu U + U^{\alpha_1} V^{\beta_1} \gamma_1 \,. \tag{5.18}$$

Here $\delta \ll 1$ and $\mu > 0$. The GM model of (1.4) corresponds to $\alpha_1 = -s$, $\alpha_2 = -q$, $\beta_1 = m$, $\beta_2 = p$, $\gamma_2 = \gamma_1 = 1$, where (p, q, m, s) satisfy (1.5). For the classical GM model where $(p, q, m, s) = (2, 1, 2, 0)$, or equivalently $(\alpha_1, \alpha_2, \beta_1, \beta_2) = (0, -1, 2, 2)$, a simple scaling analysis shows that the variables of our infinite-line GM model (5.14) and those of (5.18) are related by

$$\tau = \frac{1}{\mu} \,, \quad \varepsilon_i = \delta^2 \sqrt{\mu} \,, \quad x = \delta \sqrt{\mu} X \,, \quad t = T \,, \quad a_i = \mu^{-1/2} V \,, \quad h_i = \mu^{-1/2} U \,. \tag{5.19}$$

For other exponents sets, (5.19) still holds, except with a different relationship between a_i, h_i and V, U.

From equations (4.17), (2.40), and (2.43), of [6], the following NLEP for $\Phi(y)$ was shown to determine the stability of a one-spike solution for (5.18) on the infinite line:

$$\Phi'' - \Phi + \beta_2 w^{\beta_2 - 1} \Phi - \frac{\alpha_2 \beta_1 w^{\beta_2}}{\alpha_1 - \sqrt{1 + \lambda/\mu}} \left(\frac{\int_{-\infty}^{\infty} w^{\beta_1 - 1} \Phi \, dy}{\int_{-\infty}^{\infty} w^{\beta_1} \, dy} \right) = \lambda \Phi \,, \qquad \Phi \to 0 \,, \quad |y| \to \infty \,. \tag{5.20}$$

Here $w(y)$ is the homoclinic to $w'' - w + w^{\beta_2} = 0$. A rigorous analysis of (5.20) was given in [6]. If we take the limit $D \to 0$ in our result for the finite-domain NLEP multiplier χ_{gm} given in (2.45) of Principal Result 2.4, we obtain that $\chi_{gm} \to qm/[s + \sqrt{1 + \tau\lambda}]$. Since $\tau = \mu^{-1}$ from (5.19), and $(p, q, m, s) = (\beta_2, -\alpha_2, \beta_1, -\alpha_1)$, it follows that (5.20) agrees with our NLEP problem of Principal Result 2.4 in the limit of an infinitely long domain.

The specific following class of NLEP problems, with multiplier χ, arises in various limits of the GM and GS models:

$$\Phi'' - \Phi + 2w\Phi - \chi w^2 \left(\frac{\int_{-\infty}^{\infty} w\Phi \, dy}{\int_{-\infty}^{\infty} w^2 \, dy} \right) = \lambda \Phi \,, \qquad \chi \equiv \frac{a}{b + \sqrt{c + d\lambda}} \,, \tag{5.21}$$

for some constants a, b, c, and d. Here w is the homoclinic to $w'' - w + w^2 = 0$. As first shown in [6], and as remarked above, this class of NLEP problem occurs for a one-spike solution to the infinite line GM model. An NLEP problem of this form also arises in the intermediate regime of the GS model for periodic spike patterns (see equation (4.14) of [4]). For two-spike quasi-equilibria of the infinite-line GS model in the intermediate regime it was shown below (5.11) of §5.1 that an NLEP problem of the class (5.21) also holds, with the multiplier given by $\chi \equiv 2/[1 + \sqrt{\tau_0 \lambda}]$. An equivalent statement was first shown in equations (4.16) and (4.17) of [2] (see also Appendix A). Thus, the GS model in the intermediate regime has the key feature that each k-spike pattern is associated with exactly one universal NLEP multiplier problem.

Therefore, the cumulative results of [2], [5], and [6], show that there is an equivalence principle between the NLEP problem governing the stability of a one-spike solution for the infinite-line (classical) GM model and the NLEP problems governing the stability of two-spike quasi-equilibria or periodic spike patterns for the GS model in the intermediate parameter regime. However, our equivalence

principle expressed in Principal Result 2.5 for two spike quasi-equilibrium solutions and for equilibrium spike patterns in Proposition 3.3 of [17] is of a different nature, in that it relates the NLEP problems governing the stability of spike patterns in the finite-domain GM model to those of the GS model in the low feed-rate regime. In the equivalence principle of Principal Result 2.5 regarding two-spike quasi-equilibria, there are exactly *two* multipliers for each NLEP (i.e. $\chi_{gs\pm}$). These multipliers depend on λ in a much more intricate way than in (5.21). As we have shown, one multiplier is associated with competition instabilities and the other is associated with synchronous oscillatory instabilities.

Finally, in [9], the dynamics of two-spike quasi-equilibria were studied for the following class of reaction-diffusion equations on the infinite-line.

$$V_T = \delta^2 V_{XX} - V + g(U)V^2\,, \qquad \delta^2 U_T = U_{XX} - \delta^2\mu U + f(U)V^2\,. \tag{5.22}$$

Here $\delta \ll 1$ and $\mu > 0$. This class includes the classical GM model and various extensions of the model. In [9], an ODE was derived in equations (4.11)–(4.13) of [9] for the distance between the two spikes. Conditions for pulse-pulse attraction and repulsion were studied. For the classical GM model, where $f(U) = 1$ and $g(U) = U^{-1}$, the ODE (5.6) of [9] agrees with our result in (5.16). For a generalized GM model with $f(U) = 1$ and $G(U) = U^{-1} + \beta U^{-1/2}$, a finite-time blow-up phenomena was studied. For this model, it was shown numerically in §5.3.3 of [9] that there is a competition instability whenever the initial spike separation is below some threshold. However, the stability problem is not studied analytically. In §7.1 of [9], some qualitative remarks are made about the stability problem, and an NLEP problem of the type (5.21) was formulated in equation (7.3) of [9] for a one-spike solution.

6 Discussion

We have analyzed the dynamics and stability of one and two-spike symmetric quasi-equilibrium solutions to the GM model (1.4) and the GS model (1.3) on a finite domain. Although these two models have rather different nonlinearities, we have shown that there is an equivalence principle between them regarding both the dynamics of spikes and the mechanisms that initiate two types of spike instabilities: competition instabilities and synchronous oscillatory instabilities. Our analysis has revealed and analyzed the phenomena of dynamic instabilities, whereby slowly drifting spikes, that are initially stable on an $O(1)$ time-scale at $t = 0$, can enter an unstable zone at some point during their evolution towards an equilibrium configuration, thereby triggering the onset of a sudden competition or oscillatory instability. These dynamic instabilities were shown not to occur for the infinite-line problem. We conjecture that dynamic competition instabilities are related to the "over-crowding" instability of closely spaced spikes observed numerically in the weak-interaction regime in [35].

The analysis herein provides the first step towards an understanding of the coarsening process associated with k-spike quasi-equilibrium solutions to certain classes of reaction-diffusion systems in the semi-strong regime, that have no known variational structure. Our analysis suggests that dynamic competition and oscillatory instabilities should provide the mechanism to coarsen spike patterns and ultimately lead to a stable limiting equilibrium spike configuration. Work in this direction is in progress,

There are other open problems that should be pursued. One such problem is to give a rigorous description of the two-spike dynamics for the GS and GM models on either a bounded or an unbounded domain. Another problem is to perform a weakly nonlinear theory to investigate whether the Hopf bifurcation of the spike profile is subcritical or supercritical, and to give a rigorous proof of the uniqueness of the Hopf bifurcation value with respect to τ. From the numerical experiments in §4, our belief is that the subcritical or supercritical nature of this bifurcation is different for the GM and GS models, and may also depend on the parameters in these models. More specifically, although the linearizations of the GM model and the low feed-rate GS model are related by a spectral equivalence principle, this principle probably does not extend to the weakly nonlinear setting. A related problem is to study large-scale competition and oscillatory instabilities away from their initial onset. For the GM model, homogenization theory could be useful to analyze a one-spike evolution after the Hopf bifurcation has occurred. Finally, it would be interesting to show that dynamic competition and oscillatory instabilities are generic, in that they occur for a wide class of reaction-diffusion systems in the semi-strong interaction limit, and that they are also central instability mechanisms in a two-dimensional spatial domain.

A The Infinite-Line GS Model: Comparison With Previous Results

In [2] and [3], two-spike quasi-equilibria were analyzed for the following infinite-line GS model:

$$V_T = D_d V_{XX} - B_d V + UV^2\,, \qquad U_T = U_{XX} - UV^2 + A_d(1-U)\,. \tag{A.1}$$

A simple scaling analysis shows that the parameters of (5.1) are related to those of (A.1) by

$$\mathcal{A}_i = \varepsilon_i^{-1/2} A_i\,, \quad A_i = \frac{\sqrt{A_d}}{B_d}\,, \quad \tau = \frac{B_d}{A_d}\,, \quad \varepsilon_i^2 = \frac{D_d A_d}{B_d}\,, \quad x = \sqrt{A_d}X\,, \quad t = B_d T\,. \tag{A.2}$$

The theory of [2] and [3] involves several key groupings of parameters, which we denote here by μ, β, ω, and δ. In terms of our variables, the definition of these groupings is

$$\mu \equiv \frac{\sqrt{A_d}}{B_d} = \varepsilon_i^{1/2}\mathcal{A}_i\,, \quad \beta \equiv \sqrt{\frac{B_d^3 D_d}{A_d}} = \frac{1}{\mathcal{A}_i^2}\,, \quad \omega \equiv \sqrt{\frac{A_d D_d}{B_d^3}} = \tau\varepsilon_i^2\mathcal{A}_i^2\,, \quad \delta \equiv \sqrt{B_d D_d} = \frac{\varepsilon_i^{1/2}}{\mathcal{A}_i}\,. \tag{A.3}$$

In [2] and [3] it is assumed that $\mu \ll 1$ and $\delta \ll 1$, which implies that $\varepsilon_i^{1/2}\mathcal{A}_i \ll 1$ and $\varepsilon_i^{1/2}/\mathcal{A}_i \ll 1$. Therefore, $\mu \ll 1$ excludes the pulse-splitting regime $\mathcal{A}_i = O(\varepsilon_i^{-1/2})$, and $\delta \ll 1$ ensures that the diffusivity ratio of v to u is small. The four main parameter regimes identified in [2] and [3] are

$$\text{Case Ia: } \beta \ll 1\,,\ \omega \ll 1\,, \quad \to \quad \mathcal{A}_i \gg 1\,,\ \tau\varepsilon_i^2\mathcal{A}_i^2 \ll 1\,, \tag{A.4a}$$

$$\text{Case Ib: } \beta \ll 1\,,\ \omega = O(1)\,, \quad \to \quad \mathcal{A}_i \gg 1\,,\ \tau\varepsilon_i^2\mathcal{A}_i^2 = O(1)\,, \tag{A.4b}$$

$$\text{Case IIa: } \beta = O(1)\,,\ \omega \ll 1\,, \quad \to \quad \mathcal{A}_i = O(1)\,,\ \tau\varepsilon_i^2\mathcal{A}_i^2 \ll 1\,, \tag{A.4c}$$

$$\text{Case IIb: } \beta = O(1)\,,\ \omega = O(1)\,, \quad \to \quad \mathcal{A}_i = O(1)\,,\ \tau\varepsilon_i^2\mathcal{A}_i^2 = O(1)\,. \tag{A.4d}$$

Case Ia of [2] and [3], along with $\mu \ll 1$ and $\delta \ll 1$, corresponds to our intermediate regime $O(1) \ll \mathcal{A}_i \ll O(\varepsilon_i^{-1/2})$, where the condition (3.32) on τ holds. In this regime, equation (3.31) of [2] gives the following spike dynamics $X = \pm\Gamma(T)$ for a two-spike quasi-equilibrium solution:

$$\frac{d\Gamma}{dT} = \frac{2A_d\sqrt{D_d}}{3B_d^{3/2}} \frac{e^{-2\sqrt{A_d}\Gamma}}{\left(1+e^{-2\sqrt{A_d}\Gamma}\right)^2}\,. \tag{A.5}$$

By using (A.2) it follows that (A.5) is equivalent to our intermediate regime ODE (5.13). In Case Ia the Hopf bifurcation threshold was also identified in [2]. It occurs in Regime Ib of [2], given by $\mu^2\delta^2 \ll D_d$ and $\mu^2 = O(\sqrt{D_d})$. In our notation this corresponds to $\tau \gg 1$ and $\tau = O(\varepsilon_i^{-2}A_i^4) = O(\mathcal{A}_i^4)$, respectively. In this regime, equation (4.22) of [2] shows that a Hopf bifurcation occurs when

$$\frac{\sqrt{D_d}}{\mu^2}\left(1+e^{-2\sqrt{A_d}\Gamma}\right)^2 \approx 0.44\,. \tag{A.6}$$

A simple calculation using (A.2) shows that (A.6) is equivalent to the leading term in (5.12). Therefore, in Case Ia our results largely reproduce those of [2]. The only minor improvement that we offer in this regime is the narrow range given in (5.10) where a competition instability occurs.

Case IIa was studied in §4.2 of [3], where the ODE (4.19) of [3] characterizes the spike dynamics for a two-spike quasi-equilibrium solution. This ODE is equivalent to our result in (5.5). However, no stability analysis for this regime is given in [3]. In Remark 4.3 of [3] it is stated that the stability analysis can be studied along the same lines as for Case Ia. In our formulation, Case IIa corresponds to the low feed-rate regime $\mathcal{A}_i = O(1)$ where Principal Result 5.1 and Proposition 5.2 show that there are two different types of instabilities: competition instabilites for closely spaced spikes, and synchronous oscillatory instabilites for τ sufficiently large for well-separated spikes. The existence of these two classes of instabilities was not discovered in [3].

Case Ib was not treated herein. It corresponds to the intermediate regime where a traveling-wave instability occurs before the initiation of a Hopf bifurcation as τ is increased. In §4.1 of [3] it was shown that this regime is associated with the birth of a traveling wave instability leading to a monotonic drift of a spike. For a one-spike equilibrium solution on a finite domain in the intermediate regime, it was shown in §5 of [19] that a traveling-wave or drift instability is initiated through a Hopf bifurcation leading to an oscillatory drift of the spike location.

Acknowledgements

M. J. W. thanks the grant support of NSERC (Canada) under grant 81541, and is most grateful to the University of Washington Applied Math group for the generous use of their computer facilities. M. J. W. would like to thank Dr. Theodore Kolokolnikov for many useful discussions.

References

[1] M. Cross, P. Hohenburg, *Pattern Formation Outside of Equilibrium*, Rev. Mod. Physics, **65**, (1993), pp. 851-1112.

[2] A. Doelman, W. Eckhaus, T. J. Kaper, *Slowly Modulated Two-Pulse Solutions in the Gray-Scott Model I: Asymptotic Construction and Stability*, SIAM J. Appl. Math., **61**, No. 3, (2000), pp. 1080-1102.

[3] A. Doelman, W. Eckhaus, T. J. Kaper, *Slowly Modulated Two-Pulse Solutions in the Gray-Scott Model II: Geometric Theory, Bifurcations, and Splitting Dynamics*, SIAM J. Appl. Math., **61**, No. 6, (2000), pp. 2036-2061.

[4] A. Doelman, R. A. Gardner, T. J. Kaper, *Stability Analysis of Singular Patterns in the 1D Gray-Scott Model: A Matched Asymptotics Approach*, Physica D, **122**, No. 1-4, (1998), pp. 1-36.

[5] A. Doelman, R. A. Gardner, T. Kaper, *A Stability Index Analysis of 1-D Patterns of the Gray Scott Model*, Memoirs of the AMS, **155**, No. 737, (2002).

[6] A. Doelman, R. A. Gardner, T. Kaper, *Large Stable Pulse Solutions in Reaction-Diffusion Equations*, Indiana U. Math. Journ., Vol. 50, No. 1, (2001), pp. 443-507.

[7] A. Doelman, T. J. Kaper, P. Zegeling, *Pattern Formation in the One-Dimensional Gray-Scott Model*, Nonlinearity, **10**, No. 2, (1997), pp. 523-563.

[8] A. Doelman, H. van der Ploeg, *Homoclinic Stripe Patterns*, SIAM J. Appl. Dyn. Systems, **1**, No. 1, (2002), pp. 65-104.

[9] A. Doelman, T. Kaper, *Semistrong Pulse Interactions in a Class of Coupled Reaction-Diffusion Equations*, SIAM J. Appl. Dyn. Sys., **2**, No. 1, (2003), pp. 53-96.

[10] T. Erneux, E. L. Reiss, L. J. Holden, M. Georgiou, *Slow Passage Through Bifurcation and Limit Points. Asymptotic Theory and Applications*, Dynamic Bifurcations (Luminy 1990), pp. 14-28, Lecture Notes in Math., **1493**, Springer, Berlin, (1991).

[11] P. Fife, "Pattern Formation in Gradient Systems", in *Handbook of Dynamical Systems*, Vol. 2, pp. 677-722, North-Holland, Amsterdam, (2002).

[12] P. Freitas, C. Rocha, *Lyapunov functionals and Stability for Fitzhugh-Nagumo Systems*, J. Diff. Eq., **169**, No. 1, (2001), pp. 208-227.

[13] A. Gierer, H. Meinhardt, *A Theory of Biological Pattern Formation*, Kybernetik, **12**, (1972), pp. 30–39.

[14] P. Gray, S. K. Scott, *Autocatalytic Reactions in the Isothermal, Continuous Stirred Tank Reactor: Oscillations and Instabilities in the System* $A + 2B \to 3B$, $B \to C$, Chem. Eng. Sci. **39**, (1984), pp. 1087-1097.

[15] D. Iron, M. J. Ward, *The Dynamics of Multi-Spike Solutions to the One-Dimensional Gierer-Meinhardt Model*, SIAM J. Appl. Math., **62**, No. 6, (2002), pp. 1924-1951.

[16] D. Iron, M. J. Ward, J. Wei, *The Stability of Spike Solutions to the One-Dimensional Gierer-Meinhardt Model*, Physica D, **150**, No. 1-2, (2001), pp. 25-62.

[17] T. Kolokolnikov, M. Ward, J. Wei, *The Stability of Spike Equilibria in the One-Dimensional Gray-Scott Model: The Low Feed-Rate Regime*, submitted, Studies in Appl. Math. (2004).

[18] T. Kolokolnikov, M. Ward, J. Wei, *The Stability of Spike Equilibria in the One-Dimensional Gray-Scott Model: The Pulse-Splitting Regime*, submitted, Physica D, (2003).

[19] T. Kolokolnikov, M. Ward, J. Wei, *Slow Translational Instabilities of Spike Patterns in the One-Dimensional Gray-Scott Model*, submitted, Interfaces and Free Boundaries, (2004).

[20] T. Kolokolnikov, M. Ward, J. Wei, *Pulse-Splitting for Some Reaction-Diffusion Systems in One-Space Dimension*, to appear, Studies in Appl. Math. (2004).

[21] E. Knobloch, "Outstanding Problems in the Theory of Pattern Formation", book chapter in *Nonlinear Dynamics and Chaos. Where Do We Go From Here?*, edited by S. J. Hogan et al., Institute of Physics Publishing, Bristol, U.K. (2003).

[22] K. J. Lee, W. D. McCormick, J. E. Pearson, H. L. Swinney, *Experimental Observation of Self-Replicating Spots in a Reaction-Diffusion System*, Nature, **369**, (1994), pp. 215-218.

[23] K. J. Lee, H. L. Swinney, *Lamellar Structures and Self-Replicating Spots in a Reaction-Diffusion System*, Phys. Rev. E., **51**, (1995), pp. 1899-1915.

[24] C. S. Lin, W. M. Ni, I. Takagi, *Large Amplitude Stationary Solutions to a Chemotaxis System*, J. Diff. Eq., **72**, No. 1. (1988), pp. 1-27.

[25] H. Meinhardt, *The Algorithmic Beauty of Sea Shells*, Springer-Verlag, Berlin, (1995).

[26] C. Muratov, V. V. Osipov, *Traveling Spike Auto-Solitons in the Gray-Scott Model*, Physica D, **155**, No. 1-2, (2001), pp. 112-131.

[27] C. Muratov, V. V. Osipov, *Stability of the Static Spike Autosolitons in the Gray-Scott Model*, SIAM J. Appl. Math., **62**, No. 5, (2002), pp. 1463-1487.

[28] C. Muratov, V. V. Osipov, *Static Spike Autosolitons in the Gray-Scott Model*, J. Phys. A: Math Gen. **33**, (2000), pp. 8893-8916.

[29] NAG Fortran library Mark 17, routine D03PCF, Numerical Algorithms Group Ltd., Oxford, United Kingdom (1995).

[30] W. Ni, *Diffusion, Cross-Diffusion, and Their Spike-Layer Steady-States*, Notices of the AMS, Vol. **45**, No. 1, (1998), pp. 9-18.

[31] Y. Nishiura, D. Ueyama, *A Skeleton Structure of Self-Replicating Dynamics*, Physica D, **130**, No. 1-2, (1999), pp. 73-104.

[32] Y. Nishiura, D. Ueyama, *Spatio-Temporal Chaos for the Gray-Scott Model*, Physica D, **150**, No. 3-4, (2001), pp. 137-162.

[33] Y. Nishiura, *Far-From-Equilibrium Dynamics*, Translations of Mathematical Monographs, Vol. 209, AMS publications, Providence, Rhode Island, (2002).

[34] Y. Nishiura, *Global Bifurcational Approach to the Onset of Spatio-Temporal Chaos in Reaction-Diffusion Systems*, Methods and Appl. of Analysis, **8**, No. 2, (2001), pp. 321-332.

[35] J. E. Pearson, *Complex Patterns in a Simple System*, Science, **216**, (1993), pp. 189-192.

[36] V. Petrov, S. K. Scott, K. Showalter, *Excitability, Wave Reflection, and Wave Splitting in a Cubic Autocatalysis Reaction-Diffusion System*, Phil. Trans. Roy. Soc. London, Series A, **347**, (1994), pp. 631-642.

[37] W. N. Reynolds, S. Ponce-Dawson, J. E. Pearson, *Dynamics of Self-Replicating Patterns in Reaction-Diffusion Systems*, Phys. Rev. Lett., **72**, (1994), pp. 2797-2800.

[38] W. N. Reynolds, S. Ponce-Dawson, J. E. Pearson, *Dynamics of Self-Replicating Spots in Reaction-Diffusion Systems*, Phys. Rev. E, **56**, No. 1, (1997), pp. 185-198.

[39] W. Sun, T. Tang, M. J. Ward, J. Wei, *Numerical Challenges for Resolving Spike Dynamics for Two Reaction-Diffusion Systems*, Studies in Appl. Math., **111**, (2003), pp. 41-84.

[40] A. Turing, *The Chemical Basis of Morphogenesis*, Phil. Trans. Roy. Soc. B, **327**, (1952), pp. 37-72.

[41] D. Ueyama, *Dynamics of Self-Replicating Patterns in the One-Dimensional Gray-Scott Model*, Hokkaido Math J., **28**, No. 1, (1999), pp. 175-210.

[42] M. J. Ward, J. Wei, *Hopf Bifurcations and Oscillatory Instabilities of Spike Solutions for the One-Dimensional Gierer-Meinhardt Model*, Journal of Nonlinear Science, **13**, No. 2, (2003), pp. 209-264.

[43] M. J. Ward, J. Wei, *Hopf Bifurcations of Spike Solutions for the Shadow Gierer-Meinhardt Model*, European J. Appl. Math., **14**, No. 6, (2003), pp. 677-711.

[44] J. Wei, *On Single Interior Spike Solutions for the Gierer-Meinhardt System: Uniqueness and Stability Estimates*, Europ. J. Appl. Math., Vol. **10**, No. 4, (1999), pp. 353-378.